https://doi.org/10.5194/cp-2021-162
Preprint. Discussion started: 14 January 2022

Climate of the Past Discussions

A 300,000 year record of cold-water coral mound build-up at the East Melilla Coral Province (SE Alboran Sea, western Mediterranean)

Robin Fentimen[1*], Eline Feenstra[1], Andres Rüggeberg[1], Efraim Hall[1], Valentin Rime[1], Torsten Vennemann[2], Irka Hajdas[3], Antonietta Rosso[4], David Van Rooij[5], Thierry Adatte[2], Hendrik Vogel[6], Norbert Frank[7], Anneleen Foubert[1]

[1] Department of Geosciences, University of Fribourg, Fribourg, CH-1700, Switzerland
[2] Institute of Earth Surface Dynamics, University of Lausanne, Lausanne, CH-1015, Switzerland
[3] Laboratory of Ion Beam Physics, ETH Zürich, Zürich, CH-8093, Switzerland
[4] Department of Biological, Geological and Environmental Sciences, University of Catania, Catania, 95128, Italy
[5] Department of Geology, Ghent University, Ghent, 9000, Belgium
[6] Institute of Geological Sciences and Oeschger Centre for Climate Change Research, University of Bern, Bern, CH-3012, Switzerland
[7] Institute of Environmental Physics, University of Heidelberg, Heidelberg, D-69120, Germany

* Present address: ENS de Lyon, 15 parvis René Descartes, BP 7000, 69342 Lyon Cedex 07, France

Correspondence to: Robin Fentimen (robin.fentimen@ens-lyon.fr)

Keywords. Benthic foraminifera, bryozoans, palaeoclimate, Holocene, Pleistocene, Levantine Intermediate Water

Abstract. This study provides a detailed reconstruction of cold-water coral mound build-up within the East Melilla Coral Province (Southeast Alboran Sea) over the last 300 ky. Based on benthic foraminiferal assemblages, macrofaunal quantification, grain size analysis, sediment geochemistry, and foraminiferal stable isotope compositions, a reconstruction of environmental conditions having prevailed in the region is proposed. The variations in planktonic and benthic $\delta^{18}O$ values indicate that cold-water coral mound build-up follows and records global climate variability. In contrast to northeast Atlantic counterparts, coral mound build-up in the southeast Alboran Sea occurs during glacial as well as during interglacial periods and at very low aggradation rates (between 1 and 10 $cm.ky^{-1}$). Environmental conditions during glacial periods, particularly during the Last Glacial Maximum, appear to better suit the ecological requirements of the erect cheilostome bryozoan *Buskea dichotoma*. We propose that *Buskea dichotoma* has an important role in the build-up of cold-water coral mounds at the East Melilla Coral Province during glacial periods. Benthic foraminiferal assemblages suggest that important terrestrial input favoured cold-water coral proliferation during interglacial periods. The existence of strong Alboran Gyres during interglacial periods, promoting mixing between surface and intermediate water masses and bottom water turbulence, was possibly beneficial for cold-water coral development. Conversely, benthic foraminiferal assemblages indicate that the seafloor received less organic matter during glacial periods. Overall, the arid continental conditions combined to more stratified water masses resulted in limited coral proliferation during glacial times.

https://doi.org/10.5194/cp-2021-162
Preprint. Discussion started: 14 January 2022

Climate of the Past Discussions

1. Introduction

Cold-water coral (CWC) reefs are diverse marine ecosystems that are common on Earth (Freiwald et al., 2004; Roberts et al., 2009). The most important reef building CWC species in the Atlantic Ocean and Mediterranean Sea are the scleractinian species *Desmophyllum pertusum* (formerly known as *Lophelia pertusa*, see Addamo et al., 2016) and *Madrepora oculata* (Roberts et al., 2009). These predominantly suspension-feeding organisms depend on enhanced hydrodynamic regimes that provide food to their polyps (White et al., 2005; Mienis et al., 2007; Carlier et al., 2009; Davies et al., 2009; Roberts et al., 2009; Hanz et al., 2019). The role of internal waves (i.e., waves that occur at the interface between two water masses of different densities) on the proliferation of CWCs is important, since these oscillations increase turbulence and hence nutrient supply (White et al., 2005; Davies et al., 2009; Pomar et al., 2012; Wang et al., 2019). Physico-chemical properties of the ambient water (e.g., salinity, temperature, dissolved oxygen concentrations, pH, density) also affect CWC growth (Freiwald et al., 2004; Dullo et al., 2008; Davies and Guinotte, 2011; Hanz et al., 2019). If favourable conditions are maintained over longer periods, successive reef generations may build CWC mounds through the interaction between coral growth and sediment accumulation (Wilson, 1979; Roberts et al., 2006; Foubert and Henriet, 2009; Roberts et al., 2009). Consequently, CWC mounds can reach considerable heights of over 300 m and spread for kilometres in width and length at their base (De Mol et al., 2002; Kenyon et al., 2003; Huvenne et al., 2005). Mound development may span from thousands to millions of years and attain important mound aggradation rates, e.g., 290 $cm.ky^{-1}$ in the Porcupine Seabight (Frank et al., 2009; López Correa et al., 2012; Stalder et al., 2015; Wienberg et al., 2018). As such, CWC mounds are valuable environmental and climate archives, although mound formation is generally discontinuous (Rüggeberg et al., 2007; Roberts et al., 2009). Moreover, the sensitivity of CWCs to climate change is useful to monitor variations in environmental conditions (e.g., water mass variability, surface productivity, bottom current velocity; Rüggeberg et al., 2007; Huvenne et al., 2009; Hebbeln et al., 2016; Wienberg et al., 2018; 2020).

The long-term development of CWC mounds was first studied in the Northeast Atlantic Ocean, where it is driven by large-scale changes in oceanographic conditions (e.g., De Mol et al., 2002; Dorschel et al., 2005; Frank et al., 2011, Wienberg et al., 2018; 2020). Corals along the Irish margin grow during interglacial and interstadial times, whilst they decline during glacial periods (Dorschel et al., 2005; Kano et al., 2007; Rüggeberg et al., 2007; Eisele et al., 2008). Cold-water coral mound development along the Irish margin depends on the strength of southern-sourced water masses like the Mediterranean Outflow Water (MOW) or the Eastern North Atlantic Water (ENAW) and the formation of internal waves (White, 2007; Mohn et al., 2014; Raddatz et al., 2014; Hebbeln et al., 2016; Wienberg et al., 2020). The strong influence of the MOW during interglacial and interstadial times and the resulting enhanced turbulence induced by internal waves provides the correct balance between nutrient and sediment supply (Mohn et al., 2014; Raddatz et al., 2014). In contrast, during glacial times, weak MOW flow lowers nutrient supply and increases sediment smothering, causing coral retreat (Dorschel et al., 2005; Rüggeberg et al., 2007; Mohn et al., 2014). In the NW Atlantic Ocean, CWC mounds also form during interglacial periods, when stronger hydrodynamic regimes and better-oxygenated waters dominate the region (Matos et al., 2015; 2017). At lower latitudes in the East Atlantic, off the coast of Mauritania and in the Gulf of Cádiz, coral mounds form essentially during glacial times

https://doi.org/10.5194/cp-2021-162
Preprint. Discussion started: 14 January 2022

(Wienberg et al., 2009; Eisele et al., 2011), although they also developed at lower aggradation rates during the last interglacial (Marine Isotope Stage 5; Wienberg et al., 2018).

In the Mediterranean Sea, CWC mound provinces are concentrated in the East Alboran Sea (Fink et al., 2013; 2015; Lo Iacono et al., 2014; Stalder et al., 2015; 2018; Terhzaz et al., 2018; Wang et al., 2019; Fentimen et al., 2020a; Rachid et al., 2020; Corbera et al., 2021). The largest CWC mound field in this region is the Melilla Mound Field, covering an area greater than 500 km^2 parallel to the margin (Comas and Pinheiro, 2010; Lo Iacono et al., 2014). It can be divided into two provinces, the West and East Melilla Coral Provinces (WMCP and EMCP), respectively situated 7 km northwest and 35 km northeast of the Cape Tres Forcas (Lo Iacono et al., 2014; Fig. 1). Mound aggradation rates in the WMCP and EMCP reach their highest values (75-420 $cm.ky^{-1}$) during the Early Holocene and Bølling-Allerød interstadial. In contrast, mound formation halted during the Younger-Dryas, demonstrating low mound aggradation rates (30-50 $cm.ky^{-1}$; Fink et al., 2013; Stalder et al., 2015; Wang et al., 2019). Based on benthic foraminiferal assemblages, Stalder et al. (2015) suggest that cold/dense well-oxygenated bottom water conditions favoured CWC development, whilst Wang et al. (2019) relate the intensified coral proliferation to high surface productivity combined with strong turbulence induced by internal waves.

Although the development of coral communities at the EMCP during the last 30 ky is well documented, the long-term development and environmental forcing affecting these CWC mounds remain unknown. The aims of this study are: 1) to constrain the influence of climate variability on CWC mound formation in the EMCP over the last 300 ky, and 2) to assess long-term CWC mound formation in the area and compare it to North Atlantic counterparts.

2. Study area

2.1 Geological setting

The Alboran domain is structurally complex and its geodynamics are still debated (Duggen et al., 2008). Extension and subsidence occurred during the Early to Middle Miocene (Comas et al., 1999; Faccenna et al., 2004; Do Couto et al., 2016). The Alboran Sea is the westernmost basin of the Mediterranean Sea, and is closely connected to the Atlantic Ocean by the Strait of Gibraltar. It is approximately 400 km long, with a width of 200 km, an average depth of 1300 m and a maximum depth of 1800 m (Olivet et al., 1973; Comas et al., 1999). The Alboran Sea's metamorphic basement is intruded by a number of volcanic plateaus and seamounts formed through the extensional processes that took place between 17 and 8 million years ago (Comas et al., 1999; Duggen et al., 2008). One of these shallow volcanic plateaus, the Banc des Provençaux (ca. 200 m depth), extends in a series of 3 ridges colonized by CWCs, named "Brittlestar ridges" (BRI, BRII, BRIII) (Comas et al., 2009; Fink et al., 2013). They are part of the larger EMCP nestled at depths between 250 and 450 m. The ridges are 3 to 20 km in length, whilst the mounds vary in height from 50 to 150 m (Hebbeln et al., 2019). These mounds have mostly dead corals with scarce living corals at their summits and erosional moats at their base, supporting the presence of dynamic currents in the area (Hebbeln et al., 2019) (Fig.1).

https://doi.org/10.5194/cp-2021-162
Preprint. Discussion started: 14 January 2022

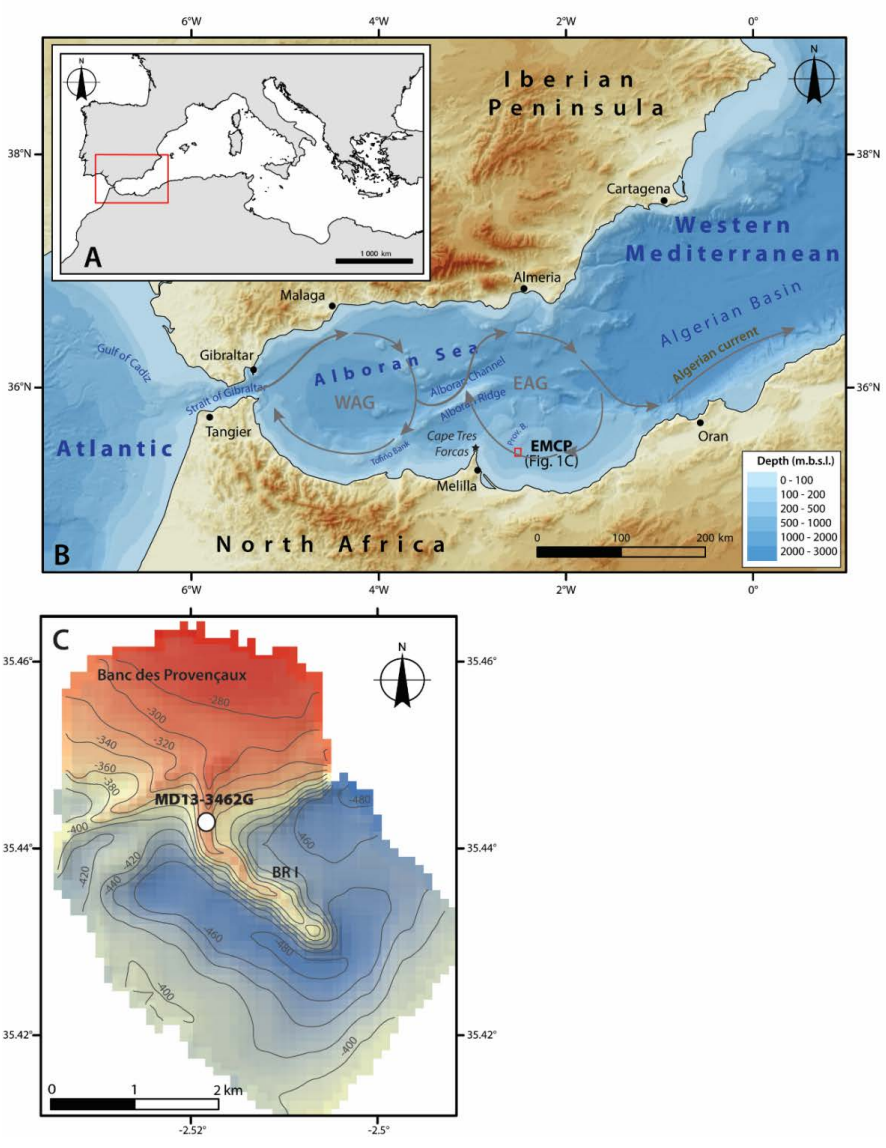

Figure 1. Location of the study area. (A) General map of the Mediterranean Sea and location of the investigated region (B) Bathymetric map of the western Mediterranean Sea based on the GEBCO_2019 gridded bathymetric data. EMCP: East Melilla Coral Province (red box); WAG: Western Alboran Gyre; EAG: Eastern Alboran Gyre. (C) Bathymetry and location of the Banc des Provençaux and Brittlestar Ridge I (BRI). The white dot indicates the location of the studied core MD13-3462G recovered during cruise "GATEWAY" No. 194 on board the research vessel *Marion Dufresne II* (Van Rooij et al, 2013).

https://doi.org/10.5194/cp-2021-162
Preprint. Discussion started: 14 January 2022

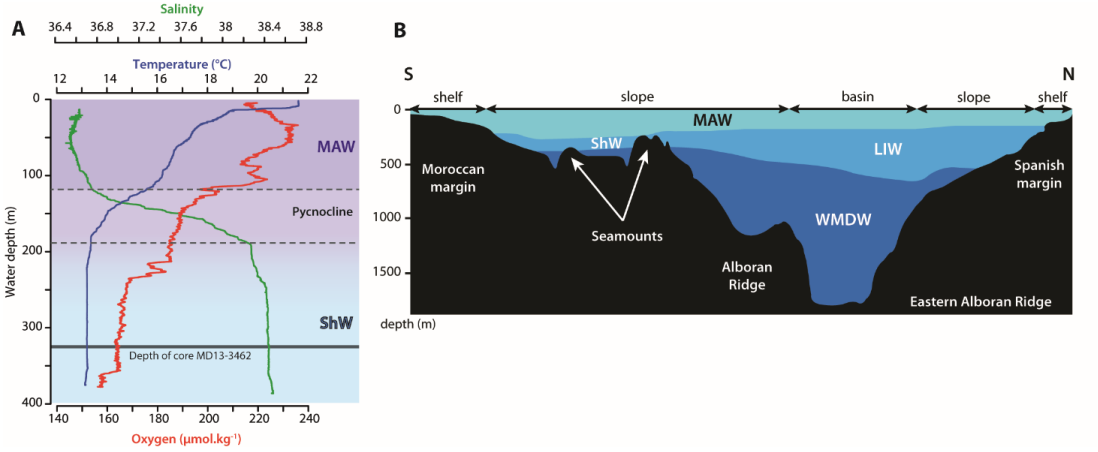

Figure 2. (A) CTD profile taken at the east of Brittlestar Ridge I (35°26,087'N; 2°30,100'W) during cruise "GATEWAY" (No. 194) on board the research vessel *Marion Dufresne II* in June 2013 (Van Rooij et al., 2013). Salinity, temperature (°C) and oxygen content (µmol.kg-1) are indicated. The location of core MD13-3462G in relation to the profile is indicated by the black line. (B) North-South orientated bottom water profile of the East Alboran Sea modified from Ercilla et al. (2016). Abbreviations: MAW: Modified Atlantic Water, ShW: Shelf Water, LIW: Levantine Intermediate Water, WMDW: Western Mediterranean Dense Water.

2.2 Oceanography

Low salinity (ca. 36.5 psu), low density Atlantic Water enters the Mediterranean through the Strait of Gibraltar. This inflowing water mass mixes with Mediterranean water while crossing the Strait of Gibraltar to form the Modified Atlantic Water (MAW), the dominant surface water mass in the Alboran Sea (La Violette, 1983; Millot, 2009). In addition, evaporation also exceeds river runoff and precipitation; hence MAW becomes saltier and denser journeying east and finally sinks in the Levantine, Aegean, Adriatic and Liguro-Provençal sub-basins (Millot et al., 2006). Intermediate waters consist of the highly saline (ca. 38.5 psu) and warm (ca. 13.5 °C) Levantine Intermediate Water (LIW) that forms in the Levantine basin and flows from East to West, entering the western Mediterranean through the Strait of Sicily to finally exit through the Strait of Gibraltar (Millot, 2013). Levantine Intermediate Water contributes to ca. 70 % of the total outflow of Mediterranean Outflow Water (MOW; Millot, 2013) and flows between 200 and 600 m water depth, whilst the core of the LIW is situated at approximately 400 m depth (Millot, 2009).

It is important to note that the LIW receives contributions from other intermediate water masses before it enters the western Mediterranean and hence has different characteristics to the LIW in the eastern Mediterranean (Millot, 2013). Moreover, intermediate waters appear to differ between the North and South Alboran Sea (Fig. 2). The LIW flows essentially along the Spanish margin, whilst Shelf Water (ShW), i.e. a mixture of MAW and Western Mediterranean Deep Water (WMDW), dominates intermediate depths along the Moroccan margin (Ercilla et al.,

https://doi.org/10.5194/cp-2021-162
Preprint. Discussion started: 14 January 2022


Climate of the Past Discussions
Open Access
EGU

2016). Brittlestar Ridge I lies in the depth range of ShW (Fig. 2). Western Mediterranean Deep Water makes up the deepest water mass, flowing under LIW and ShW. It forms in the Gulf of Lions and flows westward to finally exit through the Strait of Gibraltar and contribute to the deeper MOW (Millot et al., 2006). In the Alboran Sea, WMDW circulates principally along the Moroccan margin (Ercilla et al., 2016).

The surface MAW extends down to approximately 200 m depth (Katz, 1972) and enters the Northwest Alboran Sea as a jet (1.6 Sv; 1 Sv = $10^6.m^3.s^{-1}$; Lanoix, 1974). This jet triggers the formation of the quasi-permanent anti-cyclonic Western Alboran Gyre that contributes to mixing between surface MAW and underlying LIW (Heburn and La Violette, 1990; Lafuente et al., 1998). When the waters of the Western Alboran Gyre reach the African coast, they separate into two branches: one flows back westward along the coast towards the Strait of Gibraltar while the other flows towards the eastern part of the basin to form the Eastern Alboran Gyre (La Violette, 1983; Viúdez and Tintoré, 1995). This second non-permanent gyre also contributes to the mixing process between surface and intermediate water masses. The Banc des Provençaux and Brittlestar Ridge I are situated in the path of the westward circulating branch of the Eastern Alboran Gyre (Lanoix, 1974; Viúdez and Tintoré, 1995; Fig. 1). The mixing between surface and intermediate water masses occurs down to ca. 300 m water depth (Heburn and La Violette, 1990). The Strait of Gibraltar is a shallow (ca. 300 m depth) and narrow (ca. 20 km wide) crossing point for entering lower salinity MAW and exiting higher salinity MOW (Heburn and La Violette, 1990; Millot, 2009). Thus, the Strait of Gibraltar plays a key role in controlling water mass exchanges between the semi-enclosed Mediterranean Sea and the Atlantic Ocean. The importance of the water exchange varies between glacial and interglacial periods as a function of sea level change. Moreover, the narrow width and depth of the Strait of Gibraltar, together with the geometry of the Alboran basin and the Coriolis force,

affects the formation, mean position and shape of the Alboran gyres (Heburn and La Violette, 1990). Thus, this will in turn affect mixing between surface and intermediate water masses in the Alboran Sea.

3. Material and methods

3.1 Sample collection

This study is based on the multiproxy analysis of gravity core MD13-3462G (35°26.531ˈN, 2°31.073ˈW; 327 m depth; 926 cm long) recovered during the EUROFLEETS cruise MD194 Gateway on board the R/V *Marion-Dufresne II* (Van Rooij et al., 2013). Cores were split frozen and sedimentary facies descriptions were made at the University of Fribourg prior to sampling. These descriptions include the detailed investigation of texture, grain-size and colour of the matrix sediment, together with the identification and assessment of the preservation state of major macrofaunal components (Fig. 3). All data was plotted using the ggplot2 package for R (Wickham, 2016; R Core Team,2018).

https://doi.org/10.5194/cp-2021-162
Preprint. Discussion started: 14 January 2022

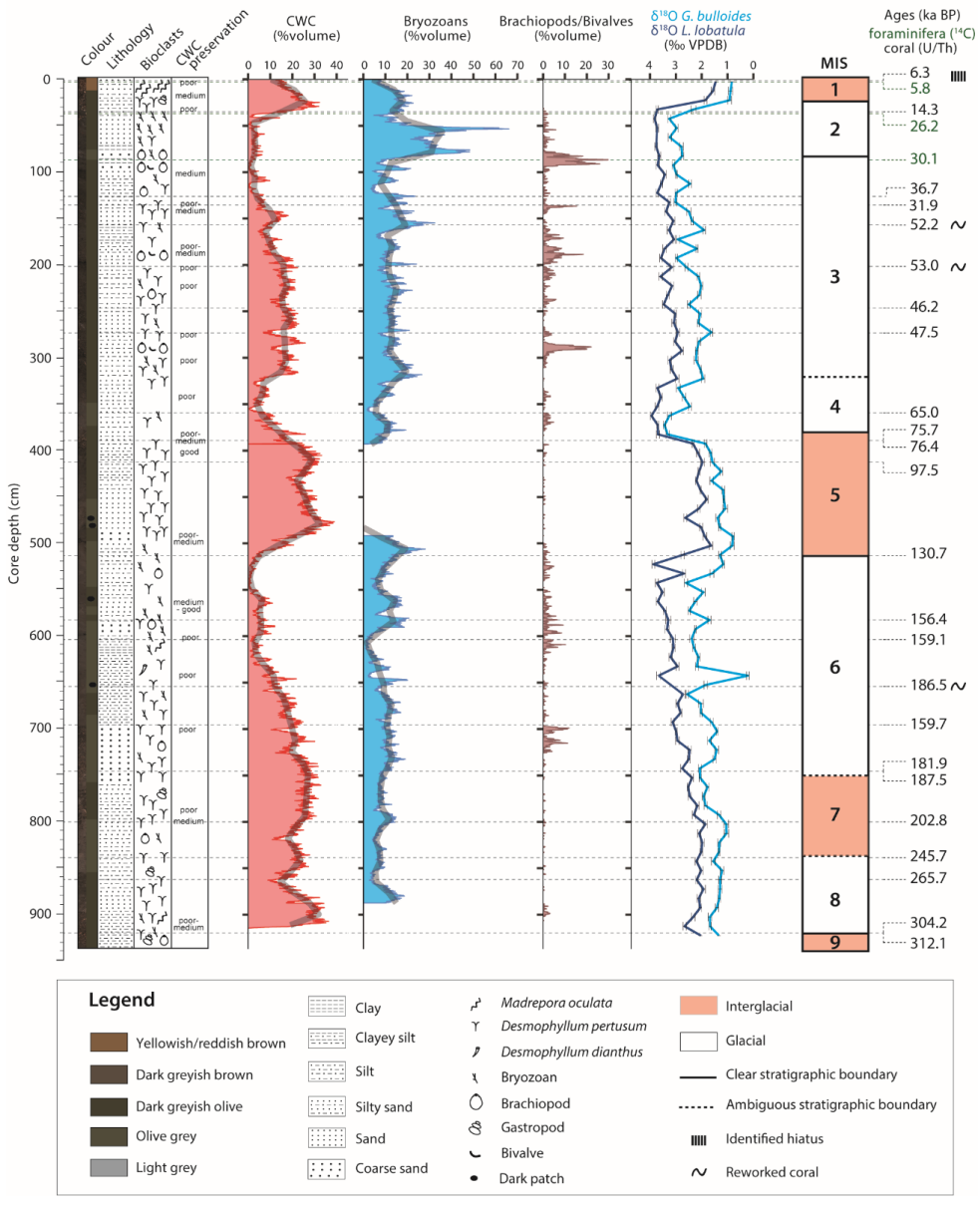

Figure 3. Core description, stratigraphy and macrofaunal composition of core MD13-3462G. Stratigraphy is based on the planktonic (*G. bulloides*) and benthic (*L. lobatula*) $\delta^{18}O$ records (‰ VPDB), the Uranium-series ages of coral fragments and the epibenthic foraminiferal radiocarbon ages for the first meter of the core (see Fig. 4).

https://doi.org/10.5194/cp-2021-162
Preprint. Discussion started: 14 January 2022


Climate of the Past Discussions

3.2 Macrofaunal quantification

X-ray Computed Tomography (CT) imaging was carried out on whole-round sections using a Siemens *Somatom Definition AS64* at the Institute of Forensic Sciences at the University of Bern (Switzerland). Core sections were scanned using an X-ray source operating at 120 kV. The images were reconstructed with a slice thickness of 0.6 mm taking into account an increment of 0.3 mm. The pixel resolution of the slices is 0.3 mm. The *Avizo 9.4* software was used to visualize, segment and quantify the volumes of the main macrofaunal components (coral, bryozoan and bivalve/brachiopod fragments). Prior to segmentation, images were filtered to remove noise in the matrix, using a non-local means filter. Brachiopods and bivalves were segmented manually. Corals, matrix, pores and bryozoans were segmented through the combination of dual thresholding and watershed segmentation. Labelled fragments smaller than 5 voxels were filtered prior to quantification. The material statistics module was used to quantify the volume % of faunal fragments per slice and the same volume of interest was selected for each core section.

3.3 Geochemical logging

Geochemical logging was performed using the *Itrax* high-resolution X-ray fluorescence (XRF) core scanner on split cores at the Institute of Geological Sciences, University of Bern (Switzerland). Measurements were taken at 5 mm intervals using an integration time of 20 s at 30 kV and 45 mA. To counter potentially biased measurements linked to the uneven surface of CWC cores, such as the direct measurement of air or of CWC skeletons, a 3-step post treatment of the dataset was carried out. First, X-ray fluorescence values with Argon counts higher than 6000, representing the measurement of air and thereby more porous/cracked media not representative of changes in matrix sediment composition, were removed from the final dataset. Secondly, each individual measurement point was compared to high-resolution core images to assess if the measurement was taken on the matrix sediment or not. Finally, elemental counts were normalized by a conservative (minor) element of the background sediment, here aluminium. Aluminium can be used effectively to counter variations in coral content (Löwemark et al., 2011). Normalization of the minor elements with Al is effective when detrital/terrestrial contribution to the sediment is high. Indeed, aluminium generally behaves conservatively and can hence be used to assess the relative variations of specific elements in sedimentary records (Calvert and Pedersen, 2007; references therein; Löwemark et al., 2011; Rodrigo-Gamiz et al., 2011; Martinez-Ruiz et al., 2015)

In this study, we use the Log_{10} normalized (Gregory et al., 2019) Si/Al and Rb/Al ratios as proxies for terrestrial (fluvial and aeolian) input. Si/Al has been used to track variations in terrestrial input since the Saharan region, which is the dominant source of aeolian dust in the Mediterranean Sea, is essentially composed of silicates with high quartz content (Guieu and Thomas, 1996; Caquineau et al., 1998; 2002) and that biogenic silica is rare in Alboran sediments (Masqué et al., 2003). Rubidium has regularly been utilized as a proxy for terrestrial run-off in the Western Mediterranean because it is often found in aluminosilicate minerals commonly encountered in fluvial material in the region (Calvert and Pedersen, 2007; Croudace and Rothwell, 2015 and references therein; Martinez-Ruiz et al.,

https://doi.org/10.5194/cp-2021-162
Preprint. Discussion started: 14 January 2022


Climate of the Past Discussions

214 2015). In combination with information provided by benthic foraminiferal assemblages, Log_{10} normalized Si/Al and
215 Rb/Al ratios hence provide valuable indications of terrestrial input.

216 **3.4 Grain-size analysis and organic geochemistry**

217 Grain-size of the siliciclastic fraction was analysed using the *Malvern Mastersizer 3000* at the Department of
218 Geology, Ghent University (Belgium). The core was sampled with a small spoon (1 cm^3) every 5 cm. Large clasts
219 (>1 cm), such as coral or bryozoan fragments, were sieved out prior to analysis. Samples were placed in 35 % H_2O_2
220 to remove organic matter and boiled until the reaction ended. Following this first step, samples were boiled in 10 %
221 HCl for 2 minutes to dissolve $CaCO_3$. Prior to measurement, samples were placed in 2 % sodium polymetaphosphate
222 and boiled to assure complete disaggregation. Any remaining particle larger than 2 mm was sieved out before
223 measurement. Eighty-seven size classes were measured (from 0.01 to 2000 µm). Each sample was measured three
224 times and results were then averaged. Mean grain-size of the siliciclastic fraction $\overline{GS}$ (Folk and Ward, 1957) was
225 calculated on the entire dataset with the *Rysgran* package for R (Gilbert et al., 2015; R Core Team, 2018). The
226 sortable silt mean size $\overline{SS}$, as defined by McCave et al. (1995; i.e., the mean of the 10-63 µm grain size range), was
227 also calculated following the same procedure. Furthermore, following McCave and Hall (2006), the percentage of
228 sortable silt (SS%) in the total <63 µm fraction was calculated. This percentage, together with the sortable silt mean
229 size, was used as an indication of bottom current velocity (McCave and Hall, 2006; Toucanne et al., 2012). It has to
230 be mentioned that the use of $\overline{SS}$ as a proxy for bottom current velocity on cores recovered from CWC mounds may
231 be biased (e.g. Eisele et al., 2011). Indeed, the baffling effect of coral framework can locally reduce bottom current
232 velocity and favour the deposition of fine sediments (Huvenne et al., 2009; Titschack et al., 2009; Fentimen et al.,
233 2020b), thus leading to an underestimation of $\overline{SS}$ during periods with high CWC content. Because of this, only
234 relative increases in $\overline{SS}$ are considered in combination with results obtained from other proxies.
235
236 Total Organic Carbon (TOC, weight%) and Mineral Carbon (MinC, weight%) contents were determined on matrix
237 sediments every 10 cm using the Rock-Eval6 technique at the laboratory of Sediment Geochemistry at the University
238 of Lausanne (Fantasia et al., 2019). The RockEval6 technique produces an Oxygen and Hydrogen index, respectively
239 corresponding to the quantity of CO_2 relative to TOC and the quantity of pyrolyzable organic compounds relative to
240 TOC (Fantasia et al., 2019). These two indices give an indication about the origin of the organic matter present in the
241 samples (Van Krevelen, 1993).

242 **3.5 Microfaunal and macrofaunal investigations**

243 The core was sampled (sliced) every 10 cm for micropaleontological analysis. Samples were weighed dry, washed
244 through a 63 µm mesh sieve and dried at 30 °C. Each fraction was then dry sieved through a series of 63, 125 and
245 2000 µm mesh sieves and weighed. A target number of 300 benthic foraminifera were identified from the fraction
246 larger than 125 µm for each sample. If the residue contained more than 600 specimens, it was split using a dry
247 microsplitter. Relative abundances (percentages) of benthic species were calculated from the total benthic
248 foraminiferal assemblage. The benthic foraminiferal density was calculated by dividing the total number of

https://doi.org/10.5194/cp-2021-162
Preprint. Discussion started: 14 January 2022


Climate of the Past Discussions

foraminifera of a given sample by the sample fraction's weight. The diversity Shannon index (H') was computed using the PRIMER6 software (Clarke and Gorley, 2006).

Samples prepared for micropaleontological analysis were further used to identify bryozoan species/genera at the Department of Biological, Geological and Environmental Sciences, University of Catania (Italy) on the 125 µm to 2 mm and >2 mm sized fractions. Key intervals with high bryozoan content, previously identified by CT imagery, were selected. Dominant scleractinian corals and main brachiopod and bivalve species were identified at the lowest taxonomic level possible on the >2 mm sized fraction at the Department of Geosciences, University of Fribourg (Switzerland).

3.6 Radiometric dating

Radiocarbon dating was performed on benthic foraminifera from 3 samples from the upper first meter of core MD13-3462G at the Laboratory of Ion Beam Physics, ETH Zürich, Switzerland (Table 1). The epibenthic foraminifera species *Discanomalina coronata*, *Lobatula lobatula* and *Cibicides refulgens* were picked in order to obtain between 4 and 10 mg of pure carbonate. The samples were first dissolved in phosphoric acid. The resulting extracted CO_2 was then converted to graphite and measured by Accelerator Mass Spectrometry (AMS) technique using the *MICADAS* dedicated instrument (Synal et al., 2007). Results were corrected for ^{13}C and calibrated using the Marine13 calibration curve (Reimer et al., 2013) and the software OxCal v4.2.4 (Ramsey, 2017). A reservoir age of 390 ± 80 years was applied to all ages (Siani et al., 2000).

Uranium-series dating was carried out on 24 CWC fragments (*D. pertusum* and *M. oculata*) using a multicollector inductively coupled plasma source mass spectrometer MC-ICPMS (*Thermo Fisher Scientific Neptune^{plus}*) coupled with a dissolver (*Aridus I*) at the Institute of Environmental Physics, Heidelberg University (Table 2). In order to constrain the chronostratigraphy of the core, well-preserved coral fragments were selected at the upper and lower boundaries of coral-rich units. These were identified based on visual core descriptions and CT-analysis (macrofaunal quantification; Fig. 3). Coral fragments were physically cleaned with a *Dremel®* drill tool and by sand blasting, and further chemically cleaned using a weak acid leaching prior to measurements. The detailed sample protocol is described by Frank et al. (2004), while spectrometry and chemical U and Th extraction and purification followed Wefing et al. (2017). Uranium-series coral ages were used to calculate mound aggradation rates.

3.7 Oxygen and Carbon stable isotope analysis

Stable oxygen and carbon isotope compositions were measured on 5 to 12 specimens of the planktonic foraminifera *Globigerina bulloides* and the benthic foraminifera *Lobatula lobatula* from the size fraction 212-250 µm in order to prevent any ontogenic effect on the measurements (Schiebel and Hemleben, 2017). The specimens were first cleaned three times with distilled water in an ultrasonic bath for 2 seconds. The measurements were then made using a *Thermo Fisher Scientific GasBench II* connected to a *Thermo Finnigan Delta Plus XL* isotope ratio mass spectrometer at the Stable Isotope Laboratory of the University of Lausanne (Switzerland) according to the method

https://doi.org/10.5194/cp-2021-162
Preprint. Discussion started: 14 January 2022

Climate of the Past Discussions
Open Access
EGU

adapted from Spötl and Vennemann (2003). Results are reported in the conventional δ-values in permil (‰) relative to the Vienna Pee Dee Belemnite (VPDB) standard. Analytical standard deviations (1σ) average 0.04 ‰ for $\delta^{13}C$ and 0.06 ‰ for $\delta^{18}O$ values based on 8 replicate analyses of standards in each sequence of 40 samples.

LAB ID	Depth (cm)	^{14}C age (BP)	±1σ	2σ lower (cal years BP)	2σ upper (cal years BP)	2σ median (cal years BP)
ETH-87743	2	5777	25	5580	5920	5760
ETH-87744	37	22811	78	25970	26530	26220
ETH-87745	87	27587	124	30730	31160	30950

Table 1. Radiocarbon ages of epibenthic foraminifera (species selected: *Lobatula lobatula*, *Cibicides refulgens* and *Discanomalina coronata*). Ages are corrected for a reservoir age of 390 ± 80 years (Siani et al., 2000).

LAB ID	Depth (cm)	S[(1)]	Age (ka)	±	Age[(2)] (ka)	±	^{238}U (µg/g)	±	^{232}Th (ng/g)	±	$\delta^{234}U$ (‰)	±	$\delta^{234}U_i$[(3)] (‰)	±
IUP- 8500	3	*M*	6.34	0.029	6.32	0.030	4.3377	0.00037	0.4311	0.00140	147.22	0.66	149.88	0.67
IUP- 8501	36	*D*	14.31	0.047	14.30	0.049	3.4367	0.00012	0.3254	0.00084	145.33	0.64	151.33	0.67
IUP- 10994	126	*D*	37.16	0.085	36.70	0.25	3.8667	0.00013	7.166	0.01328	121.99	0.51	135.30	0.57
IUP- 10995	136	*D*	35.53	0.10	31.9	1.3	3.4727	0.00015	36.120[(5)]	0.06103	126.57	0.46	138.49	0.73
IUP- 8503	158	*D*	52.57	0.19	52.24	0.22	3.7330	0.00013	4.8320	0.01200	123.72	0.83	143.41	0.96
IUP- 9310	201	*D*	53.07	0.12	53.04	0.13	2.6348	0.00008	0.3418	0.00059	126.01	0.45	146.39	0.53
IUP- 10996	248	*D*	46.33	0.12	46.20	0.13	3.5899	0.00012	1.8802	0.0029	122.48	0.60	139.53	0.69
IUP- 10997	272	*D*	47.57	0.11	47.49	0.12	3.6971	0.00013	1.1538	0.0022	121.93	0.47	139.42	0.54
IUP- 10998	360	*M*	65.39	0.17	64.96	0.28	3.5499	0.00014	6.0720	0.0084	114.78	0.46	137.87	0.56
IUP- 8504	390	*D*	76.44	0.29	76.43	0.29	3.6896	0.00011	0.1328	0.00039	115.92	0.67	143.86	0.84
IUP- 9183[a]	390	*D*	75.66	0.20	75.65	0.17	3.7004	0.00016	0.1763	0.00046	117.75	0.49	145.83	0.61
IUP- 9312	412	*D*	97.58	0.23	97.54	0.24	3.6265	0.00012	0.4572	0.00069	112.50	0.61	148.21	0.81
IUP- 9313	507	*D*	130.7	0.45	130.7	0.46	3.4073	0.00015	0.3844	0.00072	105.96	0.85	153.30	1.25
IUP- 10999	583	*D*	156.48	0.74	156.38	0.74	3.4985	0.00014	1.3288	0.0024	91.46	0.53	142.19	0.87
IUP- 10100	604	*D*	159.17	0.69	159.13	0.69	3.5045	0.00013	0.6366	0.0011	92.98	0.55	145.69	0.90
IUP- 10101	654	*D*	186.50	0.87	186.48	0.87	3.7106	0.00013	0.3339	0.00063	84.77	0.44	143.48	0.81
IUP- 10102	697	*M*	159.76	0.52	159.65	0.52	4.3503	0.00017	1.9141	0.0027	87.58	0.38	137.42	0.62
IUP- 8505	748	*D*	194.8	1.40	187.5	4.2	3.5659	0.00220	102.38[(5)]	0.27000	95.01	0.84	161.40[(4)]	2.40
IUP- 9184	756	*D*	181.9	0.79	181.9	0.78	2.8694	0.00013	0.6018	0.00099	102.72	0.79	171.74[(4)]	1.40
IUP- 10103	801	*D*	203.07	0.98	202.84	0.98	2.8444	0.00010	2.6095	0.0036	85.04	0.55	150.74	1.05
IUP- 10104	840	*D*	245.7	1.50	245.70	1.5	3.0611	0.00011	0.2657	0.00048	78.14	0.41	156.32	1.03
IUP- 9314	862	*D*	265.7	2.10	265.7	2.4	3.4662	0.00018	0.6693	0.00150	70.40	1.10	149.10	2.60
IUP- 8507	921	*D*	304.2	4.80	304.2	4.9	3.0370	0.00012	0.1176	0.00044	63.32	0.68	149.60	2.60
IUP- 9185[b]	921	*D*	312.1	3.40	312.1	3.0	3.3567	0.00016	0.2789	0.00061	58.58	0.77	141.50	2.20

https://doi.org/10.5194/cp-2021-162
Preprint. Discussion started: 14 January 2022

Climate of the Past Discussions

Table 2. Uranium-series isotope measurements (U/Th) carried out on 24 coral fragments. All errors are 2σ of the mean analytical uncertainty. Ratios determined using a Th-U spike calibrated to a secular equilibrium reference material (HU-1 at the IUP). Uncorrected, closed-system age calculated using the decay constants of Jaffey et al. (1971) for ^{238}U and Cheng et al. (2000) for ^{230}Th and ^{234}U. Ages are reported relative to the date of analysis, from year 2017 (IUP-8500 to IUP-8507) and year 2018 (other samples), and do not include uncertainties associated with decay constants. (1) Coral species: *M*: *Madrepora oculata*; *D*: *Desmophylum pertusum*. (2) Ages corrected for the contribution of initial ^{230}Th based on an estimated seawater ($^{230}Th/^{232}Th$) activity ratio of 8 ± 4. (3) Typical $\delta^{234}U_i$ reconstructed from corals for the past 30 kyr range between 135 and 155 (Chen et al., 2016). (4) Compared to the present-day seawater value of 146.8 ± 0.1 ‰, possibly indicative of U-series open system behaviour. (5) Samples containing strong residual amounts of non-carbonate contamination leading to high ^{232}Th concentrations and thus age corrections. [a] Replicate of IUP-8504; [b] replicate of IUP-8507.

4. Results

4.1 Chronostratigraphy

The chronostratigraphy of core MD13-3462G is based on the combination of the coral ages (U-series dating), the planktonic and benthic stable oxygen isotope records, and the foraminiferal radiocarbon ages for the top first meter of the core (Figs 3 and 4). The U-series coral ages indicate that core MD13-3462G extends approximately from 300 ka BP (Marine Isotope Stage 9) to the Holocene (Figs 3 and 4, Table 2). Coral ages have been widely used to define the chronology of cores recovered from coral mounds. This approach provides satisfying results although age reversals down core have to be taken into account (e.g., Rüggeberg et al., 2007; Frank et al., 2009; Matos et al., 2017). Indeed, reefs are fragile structures and can collapse, topple and fragment through the action of bioerosion, strong bottom currents, and gravity-driven processes, resulting in transport and redeposition of coral fragments (Beuck et al., 2005; Dorschel et al., 2007; White, 2007). In contrast, constructing a continuous age model based on stable isotope records is generally considered untrustworthy for cores collected from coral mounds since sedimentation is intermittent (Dorschel et al., 2005). However, coral ages at the upper and lower boundaries of coral build-up phases in core MD13-3462G (e.g., at 390 and 507 cm depth) correspond to changes in the stable oxygen isotope records (Fig. 3), which in turn match the changes between Marine Isotope Stages (MIS; Lisiecki and Raymo, 2005). As such, the stable oxygen isotope records can, in the case of core MD13-3462G and in conjunction with coral ages, indicate important stratigraphic boundaries (Fig. 4). This is particularly relevant during times when CWCs did not grow and hence cannot serve to construct a timeframe. Stable oxygen isotope records were hence correlated to the reference LR04-stack (Lisiecki & Raymo, 2005) for the $\delta^{18}O$-stratigraphy (see Fig. 4a). Tie points were identified using Lineage in the software package AnalySeries v. 2.0.8 (Paillard et al., 1996; Table 3). A clear subdivision into glacial–interglacial stages and substages was possible for Marine Isotope Stages (MIS) 1 to 6 with a correlation coefficient of R^2 = 0.61, being in good agreement with the CWC U-series age dates (see Fig. 4b). However, the correlation became difficult below 520 cm core depth due to the resolution of sampling (= 10 cm), the lower sedimentation rate and possible

https://doi.org/10.5194/cp-2021-162
Preprint. Discussion started: 14 January 2022

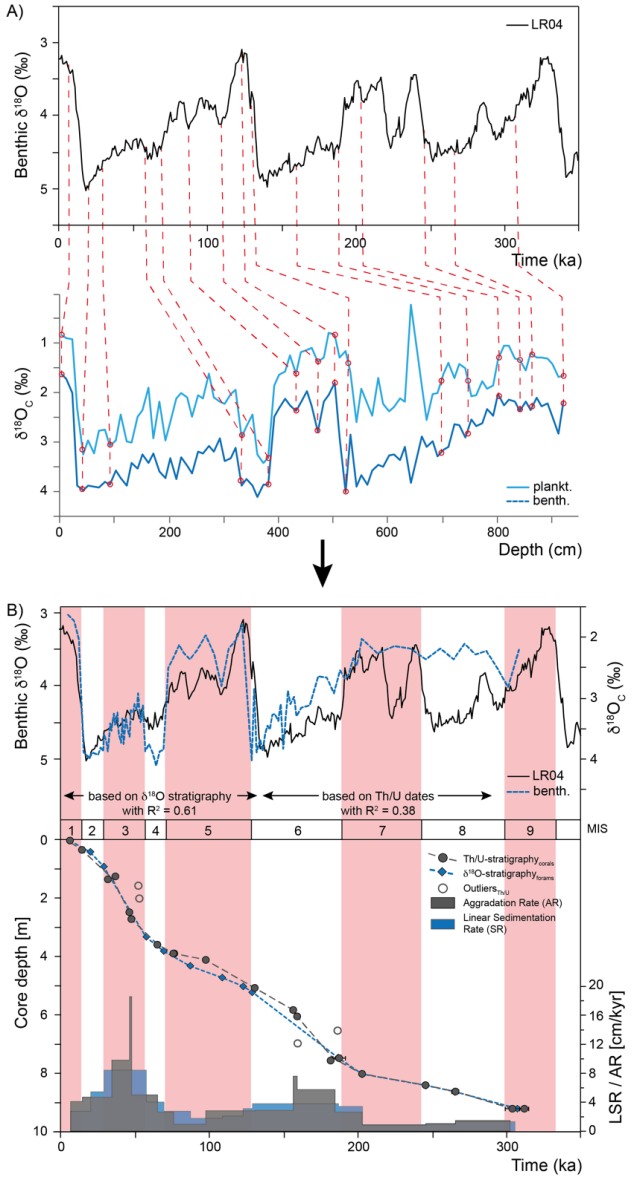

Figure 4. (A) Correlation pointers (see Table 3) between LR04 benthic $\delta^{18}O$ stack of Lisiecki and Raymo (2005) and the benthic (*L. lobatula*) and planktonic (*G. bulloides*) $\delta^{18}O$ record of MD13-3462G. (B) The $\delta^{18}O$ stratigraphy has good correlation for the younger part (MIS 1–5, R^2 = 0.61), but the lower part (>MIS 6), which is based on the U-series CWC dates, has a weak correlation (R^2 = 0.38). The comparison between the U-series- and $\delta^{18}O$-stratigraphy-based age-depth correlations indicates good coherence. The resulting $\delta^{18}O$ -stratigraphy-based Linear Sedimentation Rate (LSR) may serve as an indication for changes in the sedimentary regime, but shows similar values/trends as the CWC-age-based Aggradation Rate (AR), with high rates during MIS 3, MIS 6 and late MIS 7. Marine Isotope Stages (MIS) follow boundaries defined by the LR04-stack (Lisiecki and Raymo, 2005).

https://doi.org/10.5194/cp-2021-162
Preprint. Discussion started: 14 January 2022

Climate of the Past Discussions
Open Access
EGU

337

Depth (cm) of core MD13-3462G	Time (ka) of LR04 stack	LSR (cm/ka)	
4	6.3	2.8	Top marker
42	20.0	5.5	MIS 2 peak
91	29.0	8.5	MIS 2/3
333	57.5	4.1	MIS 3/4
381	69.5	2.8	MIS 4/5
431	87.2	1.8	MIS 5.2 peak
472	108.9	2.2	MIS 5.4 peak
501	122.8	3.2	MIS 5.5 peak
522	129.1	3.9	MIS 5/6
697	159.7	3.5	Th/U date
802	203.1	0.9	Th/U date
841	245.8	1.1	Th/U date, MIS 7/8
862	265.6	1.4	Th/U date
920	307.5		Bottom marker, MIS 8/9

338

339 **Table 3.** Correlation pointers between sediment depth and time based on the benthic $\delta^{18}O$ record of core MD13-3462G and the
340 benthic LR04 stack of Lisiecki and Raymo (2005) for main Marine Isotope Stage (MIS) boundaries. The correlation coefficient
341 between the two records is 0.676. Due to possibly unidentified hiatuses the Linear Sedimentation Rate (LSR) should not be
342 considered as absolute but may serve as a guidance to indicate changes in the sedimentary regime.

343

https://doi.org/10.5194/cp-2021-162
Preprint. Discussion started: 14 January 2022

hiatuses and reworking units flattening the curve. Therefore, U-series ages were used to correlate the lower part of the core, resulting in a correlation coefficient of R^2 = 0.38 (total R^2 = 0.43). The foraminiferal $\delta^{18}O$ records still follow the LR04-stack until late MIS 7, but the signal remains at relatively light $\delta^{18}O$ values for the bottom ~100 cm of MD13-3462G covering a timespan of around 100 ka (Fig. 4b).

The stratigraphic boundaries from the base of the core to ca. 600 cm depth were defined based on the U-series coral ages as planktonic stable oxygen isotope compositions show little variation. The boundaries of MIS 8 are the most poorly defined. Due to difficulties to define precisely the stratigraphy of this section of the core, it will not be considered in detail during this study. In contrast, the planktonic and benthic $\delta^{18}O$ values and the coral ages do constrain the stratigraphic boundaries from MIS 6 to MIS 1 (Fig. 4). Contrary to sediment records from CWC mounds of the North Atlantic, where no clear glacial or interglacial $\delta^{18}O$ values are reported (e.g., Dorschel et al., 2005; Rüggeberg et al., 2007; Eisele et al., 2008; Mienis et al., 2009), core MD13-3462G presents typical interglacial and glacial $\delta^{18}O$ values of the Alborán Sea for both, planktonic (< 1 ‰ and ~3 ‰, resp.) and benthic (~1.5 ‰ and ~4‰, resp.) foraminifera (e.g., Cacho et al., 1999; Cacho et al., 2006; Stalder et al., 2015). Therefore, low planktonic and benthic $\delta^{18}O$ values correspond to interglacial periods, whilst high planktonic and benthic $\delta^{18}O$ values correspond to the two last glacial periods (Figs. 3 and 4).

4.2 Sediment characterization

The sediment in core MD13-3462G consists mostly of macrofaunal remains (essentially corals and bryozoans) surrounded by a clay- to silt-sized carbonate/siliciclastic matrix. No important variation in the matrix sediment is observed throughout the core. Total organic carbon content in the sediment varies between 0.16 and 1.13 wt% (Fig. 5). The highest TOC value is measured during late MIS 3 (1.13 wt%), whilst the lowest is recorded during MIS 8 (0.16 wt%; Fig. 5). The most important shifts to higher TOC values are observed during MIS 5, MIS 3 and at the transition between MIS 2 and MIS 1 (Fig. 5). The sediment samples are further characterized by low Hydrogen index values (< 300 mg HC/g TOC; Fig. 6), indicating that the organic matter is oxidized and of essentially terrestrial origin (Espitalié et al., 1985).

The mean sortable silt grain size of the siliciclastic fraction ($\overline{SS}$) varies between ca. 19 and ca. 26 µm (Fig. 5). Overall, a decrease in $\overline{SS}$ is marks the passage from interglacial to glacial periods. This is particularly noticeable at the transition from MIS 7 to MIS 6 were $\overline{SS}$ decreases abruptly from approximately 25 to 19 µm (Fig. 5). Conversely, an increasing trend is observed from ca. 550 to ca. 375 cm depth, corresponding to the passage from the later phases of MIS 6 to the end of MIS 5 (Fig. 5). The percentage of sortable silt (SS%) increases with $\overline{SS}$ (Fig. 7). As discussed by McCave and Hall (2006) and McCave et al. (2017), the straight-line relationship (slope of ca. 0.125 µm/% and an intercept at 0% of ca. 17.5 µm) between $\overline{SS}$ and SS% is indicative of a sorting process induced by bottom currents (Fig. 7).

https://doi.org/10.5194/cp-2021-162
Preprint. Discussion started: 14 January 2022

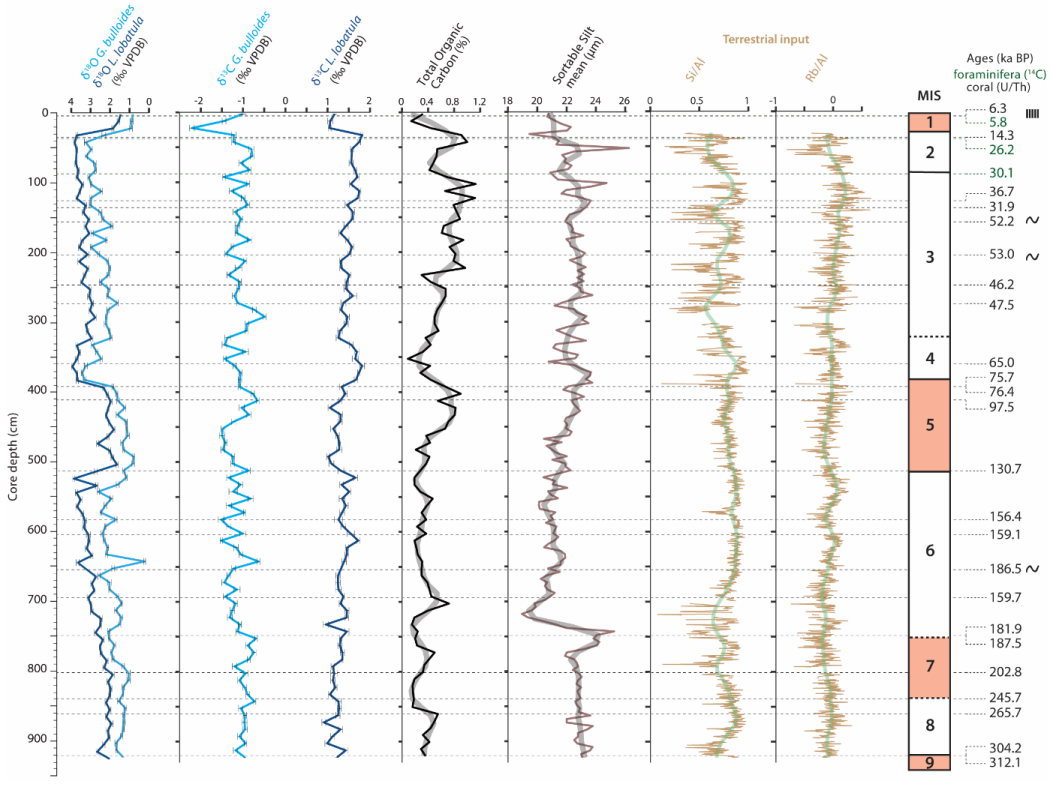

Figure 5. Planktonic (*G. bulloides*) and benthic (*L. lobatula*) $\delta^{13}C$ records, Total Organic Carbon content (%), mean grain size of the sortable silt fraction (the 10-63 μm grain size range, expressed in μm; McCave et al., 2006), and the Log_{10} titanium (Ti) and rubidium (Rb) aluminium (Al)-normalized ratios. Smoothed curves are indicated by the shaded curves. The planktonic (*G. bulloides*) and benthic (*L. lobatula*) $\delta^{18}O$ records (‰ VPDB) are provided as supporting information.

4.3 Stable carbon isotopes

The range of $\delta^{13}C$ values of the planktonic *G. bulloides* is between -2.2 ‰ at 12 cm and -0.5 ‰ at 292 cm, whereas that for the benthic *L. lobatula* is between 0.9 ‰ at 872 cm and 1.8 ‰ at 362 cm (Fig. 5). The planktonic $\delta^{13}C$ record has a higher variability compared to the benthic $\delta^{13}C$ record (Fig. 5). During MIS 6, the benthic $\delta^{13}C$ is relatively high (ca. 1.5 ‰), whilst the planktonic $\delta^{13}C$ record fluctuates between -0.6 ‰ and -1.5 ‰. A decrease in the planktonic $\delta^{13}C$ record (from -0.7 to -1.5 ‰) marks the middle of MIS 5. In contrast, the benthic $\delta^{13}C$ remains stable and low (ca. 1.2 ‰) throughout MIS 5 (Fig. 5). The passage from MIS 4 to MIS 3 is characterized by a shift from the low planktonic $\delta^{13}C$ recorded during MIS 4 (-1.5 ‰) to higher planktonic $\delta^{13}C$ (-0.5 ‰). Conversely, benthic $\delta^{13}C$ values shift from high (1.8 ‰) to lower values (1.3 ‰). The passage from MIS 2 to MIS 1 is marked by a sharp decrease in planktonic and benthic $\delta^{13}C$ (from -1.2 ‰ to -2.2 ‰ and from 1.8 ‰ to 1.0 ‰ respectively). The last two

https://doi.org/10.5194/cp-2021-162
Preprint. Discussion started: 14 January 2022

396 glacial intervals, in particular MIS 4, are marked by a stronger difference between benthic and planktonic $\delta^{13}C$
397 values (Fig. 4).

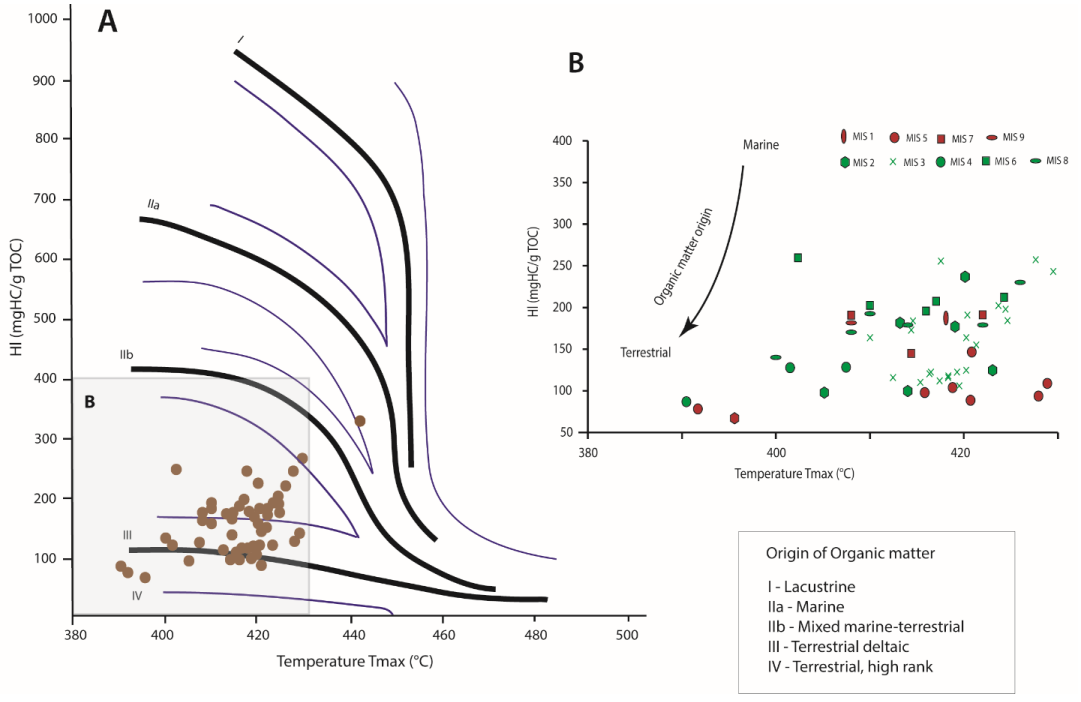

398
399

400 **Figure 6.** (A) Hydrogen Index (HI; mgHC/g TOC) vs. Tmax (°C) obtained by RockEval6 pyrolysis. (B) Close-up. The organic
401 matter origin becomes more terrestrial with decreasing HI values.
402
403
404
405

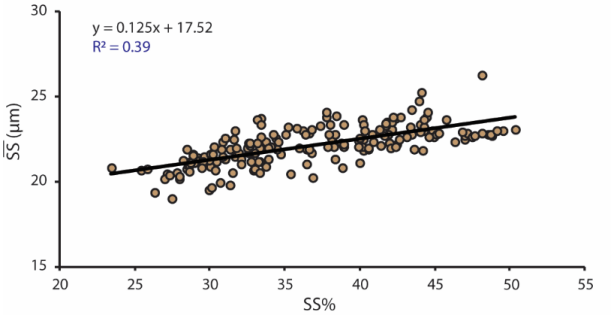

406
407 **Figure 7**. Dispersion plot of the sortable silt mean size (the 10-63 µm grain size range, expressed in µm) $\overline{SS}$ vs. the percentage of
408 sortable silt (SS%). The slope of 0.125 µm and intercept at 0 % of 17.52 µm indicates a sorting process induced by bottom
409 currents (McCave et al., 2006).

https://doi.org/10.5194/cp-2021-162
Preprint. Discussion started: 14 January 2022

410 **4.4 Elemental geochemistry**

411 Variations in Si/Al are more marked during MIS 7 and the last glacial period, in comparison with the more stable
412 values recorded during MIS 6 and MIS 5. The transitions from MIS 7 to MIS 6 and from MIS 5 to MIS 4 are
413 characterized by fluctuating Si/Al values (Fig. 5). The Rb/Al ratios demonstrate overall low values throughout the
414 core. However, higher Rb/Al ratios are reached at the end of MIS 6 and MIS 3 (ca. 100 cm). In the same way as for
415 Si/Al record, Rb/Al ratios demonstrate an important variability during MIS 7 and the last glacial period; in
416 comparison to other periods where the records are comparatively stable (Fig. 5).

417 **4.5 Macrofauna**

418 The major macrofaunal fragments present in the core are scleractinian corals, bryozoans, brachiopods and bivalves
419 (Fig. 3; Fig. 8). Sea urchins, gastropods, serpulids and gorgonian fragments are more sporadically distributed. The
420 dominant coral species in the core is the scleractinian *D. pertusum*. In the upper 20 cm, *D. pertusum* is replaced by
421 *M. oculata* (Fig. 3; Fig. 8). A third and solitary species, *Desmophyllum dianthus*, is scarcely distributed (Fig. 3).
422 High CWC content is observed during interglacial periods, whilst low content characterizes glacial periods (Fig. 3).
423 During MIS 3 coral content shows a more staggered distribution, with a range of values from less than 10 vol% to ca.
424 27 vol% (Fig. 3). The Aggradation Rate of mound sediments, determined from the coral ages, indicate higher rates of
425 6 to 8 cm/kyr during MIS 3 and early MIS 6 being well in coherence with the Linear Sedimentation Rate based on
426 the foraminifera $\delta^{18}O$-stratigraphy of the background sediment (Fig. 4B)
427
428 In total 23 genera of bryozoans were identified. *Buskea dichotoma* is by far the dominant bryozoan species (Fig. 8).
429 Accessory species/genera are mainly represented by *Reteporella sparteli*, *Tubuliporina* sp. and *Palmiskenea* sp.
430 Bryozoan content varies in general between 10 and 20 vol% (Fig. 3). Very high content is, however, observed during
431 MIS 2, reaching near to 70 vol%. The fragments, although delicate and fragile, are well preserved, large sized and
432 unworn (Fig. 8). Bryozoans are absent during most of MIS 5. This absence corresponds to the interval when coral
433 content is the most important (Fig. 3). Conversely, the maximum abundance of bryozoans during MIS 2 correlates to
434 a minimum in coral content (Fig. 3).
435
436 Brachiopods are mainly represented by the co-occurrence of the species *Gryphus vitreus* and *Terebratulina retusa*
437 (Fig. 8). These two brachiopods are regularly associated to the bivalve *Bathyarca pectunculoides* (Fig. 8). These
438 three inverterbrates have been formerly reported from Mediterranean CWC environments. *Gryphus vitreus* and
439 *Terebratulina retusa* are also recorded from Pleistocene CWC deposits from Rhodes, Greece (Bromley, 2005),
440 whilst *Bathyarca pectunculoides* was found at the Santa Maria di Leuca CWC province (Mastrototaro et al., 2010;
441 Negri and Corselli, 2016). *Gryphus vitreus* was also found associated to “white corals” between 235 and 255 m
442 depth off the coast of the Hyères Islands, France (Emig and Arnaud, 1988). Although being fragile, the shells are
443 well preserved (Fig. 8). The brachiopod/bivalves concentrate as layers and demonstrate a non-continuous distribution
444 (Fig. 3 and 8).

https://doi.org/10.5194/cp-2021-162
Preprint. Discussion started: 14 January 2022

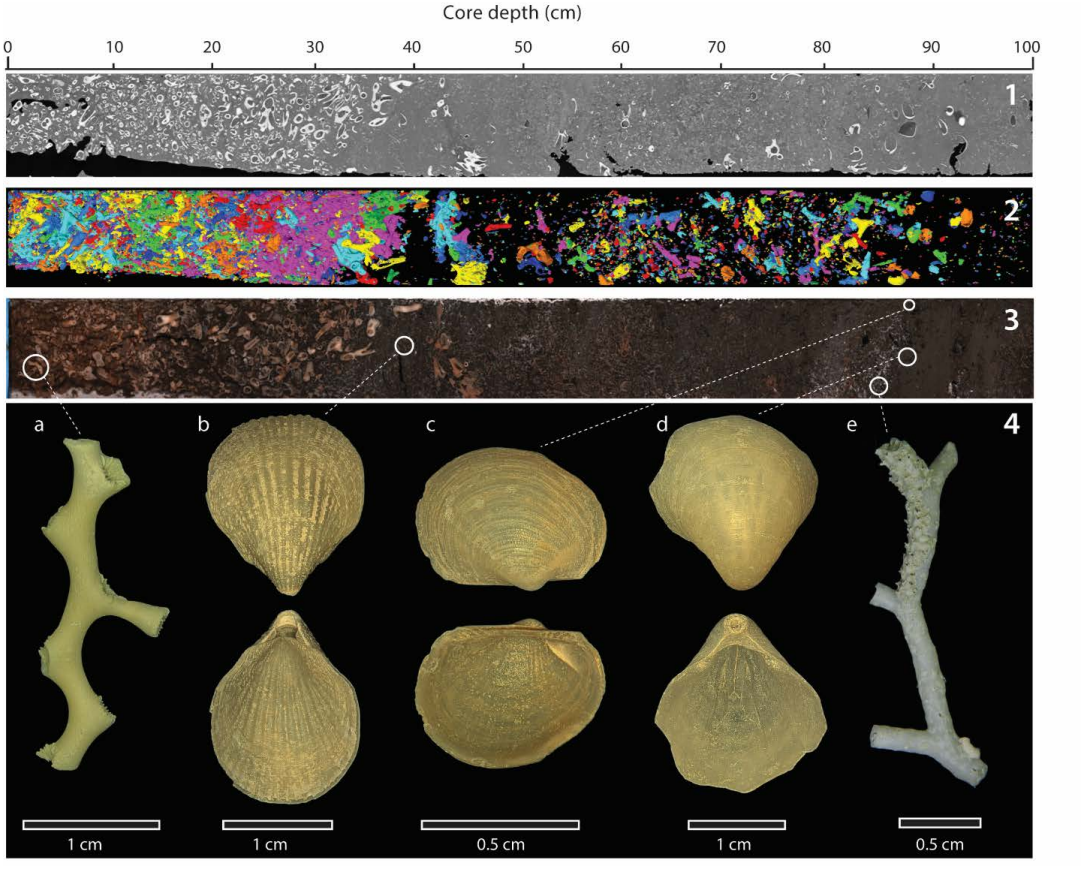

Figure 8. Example of a sediment core section showing the main macrofaunal components (section 1, 0-100 cm). (1) X-ray Computed Tomography imagery. (2) Three-dimensional reconstruction of coral fragments performed on X-ray Computed Tomography (CT) images. (3) Split-core high-resolution image. The white circles indicate the location of main macrofaunal components. (4) Main macrofaunal components: (a) the scleractinian coral *Madrepora oculata*, (b) the brachiopod *Terebratulina retusa*, (c) the bivalve *Bathyarca pectunculoides*, (d) the brachiopod *Gryphus vitreus*, (e) the bryozoan *Buskea dichotoma*.

They reach their highest abundance during glacial periods, in particular at the end of MIS 3 (30 vol% at 80 cm). Brachiopods and bivalves are completely absent during the last two interglacial periods (Fig. 3).

4.6 Benthic foraminiferal assemblages

Shannon diversity ranges between ca. 2.8 at 652 cm and 3.6 at 782 cm (Fig. 9). High Shannon diversity values between 3.4 and 3.6 are recorded during interglacial periods (Fig. 9). The lowest Shannon diversity values (between 2.8 and 3.0) are associated to glacial periods (Fig. 9). A total number of 166 benthic foraminifera species were recognized (see Supplementary material). The most abundant species are *Bolivina spathulata*, *Bulimina marginata*,

https://doi.org/10.5194/cp-2021-162
Preprint. Discussion started: 14 January 2022

460 *Bulimina striata*, *Cassidulina laevigata*, *Discanomalina coronata*, *Gavelinopsis praegeri*, *Globocassidulina*
461 *subglobosa*, *Hyalinea balthica*, *Lobatula lobatula*, *Miliolinella subrotunda*, *Trifarina angulosa* and *Uvigerina*
462 *mediterranea*.
463

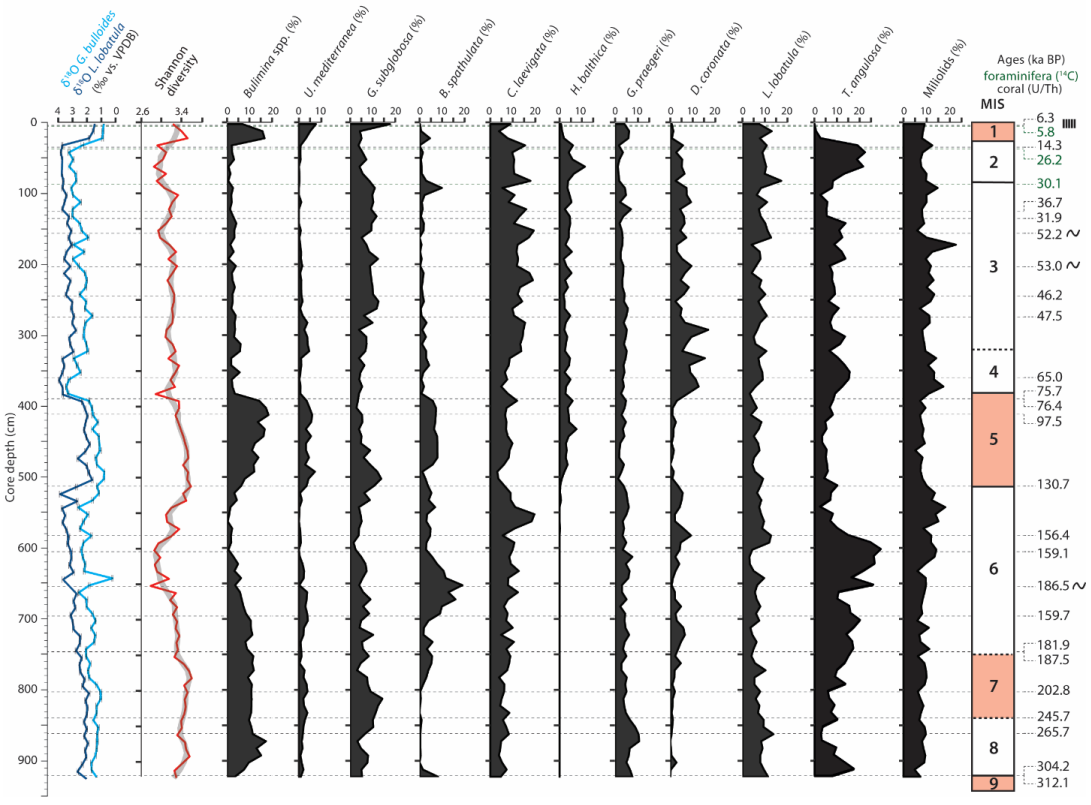

464
465
466 **Figure 9**. Distribution of main benthic foraminifera (expressed as the percentage of the total number of benthic foraminifera) and
467 benthic foraminiferal Shannon diversity (the overlaid grey curve corresponds to the smoothed curve). The planktonic (*G.*
468 *bulloides*) and benthic (*L. lobatula*) $\delta^{18}O$ records (‰, VPDB) are provided as supporting information.
469
470 The three Buliminid species *B. aculeata*, *B. marginata* and *B. striata* demonstrate the same distribution trends and
471 were thus grouped together as *Bulimina* spp. All Miliolids were grouped together for the same reason. The species
472 *M. subrotunda* makes up more than half of the total abundance of the Miliolid group with an average contribution of
473 ca. 53.4 %. The abundances of all important species are given in Figure 9. The opportunistic infaunal *Bulimina* spp.
474 show maximum abundances during interglacial periods (ca. 18 %) and minimum abundances during glacial periods
475 (ca. 2 %; Fig. 9). *Uvigerina mediterranea* follows a similar distribution to Buliminids, with peak abundances
476 corresponding to interglacial periods (Fig. 9). Relative to *Bulimina* spp., *U. mediterranea*, and *G. subglobosa*, the
477 infaunal *T. angulosa* and the epifaunal *D. coronata* are the least abundant during the last two interglacials (between

https://doi.org/10.5194/cp-2021-162
Preprint. Discussion started: 14 January 2022


Climate of the Past Discussions

ca. 1 and 5 %), whilst they are the most abundant during glacial periods, with peak abundances reached during MIS 4 for *D. coronata* (ca. 30 %; Fig. 9). Abundances of Miliolids (5-22 %), *L. lobatula* (3-17 %) and *C. laevigata* (3-17 %) are relatively high throughout the entire core (Fig. 9); although Miliolids show higher abundances during glacials (ca. 20 %). The highest numbers of *C. laevigata* are recorded during glacial periods (ca. 20 %), whilst minimum abundances occur during interglacials (3 % during MIS 5). The epifaunal *G. praegeri* is homogeneously distributed, in contrast to *H. balthica* that first appears in the core at the onset of MIS 5, reaching maximum abundances during MIS 2 (ca. 11 %; Fig. 9). The infaunal *B. spathulata* is the most abundant during MIS 6 (ca. 20 %) and reaches approximately 10 % during interglacial periods (MIS 9, MIS 7 and MIS 5; Fig. 9).

5. Discussion

5.1 Environmental controls on coral proliferation during interglacial periods

5.1.1 High food availability associated to humid continental conditions

During interglacial periods, benthic foraminiferal assemblages are marked by high abundances of the infaunal *Bulimina* spp., *U. mediterranea* and to a lesser extent *B. spathulata*. Several authors describe *Bulimina* spp. as characteristic for eutrophic and dysoxic environments (Phleger and Soutar, 1973; Lutze and Coulbourn, 1984; Jorissen, 1987; Schmiedl et al., 2000). In the Mediterranean Sea, they are dominant in the vicinity of the Po river delta in the North Adriatic Sea and close to the Rhône River delta (Jorissen, 1987; Mojtahid et al., 2009). The shallow infaunal *U. mediterranea* and the opportunistic *B. spathulata* are known to demonstrate a positive correlation with organic matter flux (De Rijk et al., 2000; Schmiedl et al., 2000; Fontanier et al., 2002; 2003; Drinia and Dermitzakis, 2010). Moreover, *Bulimina* spp. and *U. mediterranea* are reported to be able to feed on fresh but also more refractory organic matter (De Rijk et al., 2000; Koho et al., 2008; Dessandier et al., 2016). Based on these observations, the benthic foraminiferal assemblage during interglacials would support a high organic matter export to the seafloor. The overall higher TOC levels during interglacials confirm that the sediment during these periods was relatively enriched in organic matter in comparison to glacial periods (Fig. 5). High abundance of the shallow infaunal *G. subglobosa* has been linked to the deposition of fresh phytodetritus on the seafloor after bloom events (Gooday, 1993; Fariduddin and Loubere, 1997; Suhr et al., 2003; Sun et al., 2006). It is typically found in high energy (e.g. steep flanks, ridges) and well-oxygenated environments (Mackensen et al., 1995; Milker et al., 2009), and is a common taxon of the Alboran Platform and of CWC environments (Margreth et al., 2009; Milker et al., 2009; Spezzaferri et al., 2014). Mackensen et al. (1995) noted that *G. subglobosa* dominated in areas of the South Atlantic Ocean where the organic carbon flux did not exceed 1 $g.m^{-2}.yr^{-1}$. In contrast, in the Mediterranean Sea, *B. marginata* is restricted to sites with an organic carbon flux >2.5 $g.m^{-2}.yr^{-1}$, whilst *B. aculeata* is associated to a flux of 3 $g.m^{-2}.yr^{-1}$ (De Rijk et al., 2000). The last two interglacials (MIS 7 and MIS 5) are marked by an increased abundance of *G. subglobosa* at early stages followed by a general decline. Buliminids follow a converse trend, particularly during MIS 5, with lower abundances at early stages (Fig. 9). This suggests that conditions during the later stages of interglacials became increasingly eutrophic and in turn less oxygenated at the sediment/water

https://doi.org/10.5194/cp-2021-162
Preprint. Discussion started: 14 January 2022


Climate of the Past Discussions

interface, as the consumption of organic matter led to oxygen depletion. These more environmentally stressful conditions resulted in decreased foraminiferal diversity and a proliferation of opportunistic taxa (Fig. 9). Overall lower abundances of Miliolids, which are typically found in well-oxygenated environments (Murray, 2006), further confirm eutrophication coupled to lower oxygenation at the seafloor during interglacials, specifically towards the end of interglacials (Fig. 9).

Schmiedl et al. (2010) link the high abundance of *U. mediterranea* in the Aegean Sea to humid climatic conditions and increased river runoff. Increased fluvial input has been widely linked in the eastern Mediterranean to more humid continental conditions during interglacial times in response to a northern shift of the African monsoon (e.g., Gasse, 2000; Gasse and Roberts, 2005; Osborne et al., 2008; Coulthard et al., 2013). In contrast, the Alboran Sea lies below the maximum Inter-Tropical Convergence Zone northward position and is sheltered by the Atlas Mountain chain (Rohling et al., 2002; Tuenter et al., 2003; Lavaysse et al., 2009). Modern-day observations show that rainfall over the northwest Atlas Mountains is generally associated to baroclinic activity over the North Atlantic (Knippertz et al., 2003; Braun et al., 2019). The south of the Atlas Mountains has one of the highest cyclonic activities in the Mediterranean borderlands, whilst the largest fraction of cyclones entering the Mediterranean Sea arrives from the Atlantic (Lionello et al., 2016). Pasquier et al. (2018) noticed that periods of increased input of organic matter from sediment-laden rivers occur during warm substages of the last 200 ky. These authors relate these pluvial events to negative North Atlantic Oscillation-like conditions (Pasquier et al., 2018). The East Melilla Coral Province is located 50 km away from the mouth of the Moulouya River which takes its source in the High Atlas Mountains (Snousi, 2004; Emelyanov and Shimkus, 2012; Tekken and Kropp, 2012). The basin of the Moulouya River covers approximately 54,000 km^2, hence representing the largest river basin in Northwest Africa (Emelyanov and Shimkus, 2012; Tekken and Kropp, 2012). We propose that the influence of warm and moist Atlantic air masses during interglacial periods promoted warmer and more humid conditions over Northwest Africa and torrential rainfall. This would have led to a strengthening of the Moulouya River's flow rate, hence triggering episodes of important terrestrial organic matter input at BRI (Fig. 6). These events may have in turn caused eutrophication and oxygen depletion at the seafloor, compatible with the observed benthic foraminiferal assemblages (Fig. 9). Dysoxic conditions during interglacial periods would have hampered coral proliferation, as suggested by the low mound aggradation rates (Fig. 4). However, dysoxic conditions may have been limited to the sediment, thus only affecting foraminiferal communities and not fully preventing colonial corals living above the sediment surface to develop. Such vertical decoupling between sediment and pelagic ecosystems has previously been observed in modern Norwegian CWC reefs (Wehrmann et al., 2009). Overall, high food availability triggered by increased fluvial discharge appears to be a decisive parameter governing coral proliferation at BRI.

5.1.2 Enhanced surface and intermediate water mass mixing

During interglacial periods, the high sea level and the increased evaporation in the Mediterranean leads to a more important inflow of low salinity MAW through the Strait of Gibraltar (Sierro et al., 2005). Thus, surface waters in

https://doi.org/10.5194/cp-2021-162
Preprint. Discussion started: 14 January 2022


Climate of the Past Discussions

548 the Alboran Sea are, in comparison to glacial periods, warmer and less dense. This is also noticed in the planktonic
549 $\delta^{18}O$ record (Fig. 3). The enhanced MAW flow during interglacials triggers stronger Western and Eastern Alboran
550 Gyres, resulting in better mixing and downwelling. Knowing that the Banc des Provençaux and BRI are situated at
551 relatively shallow water depths and in the path of the westward circulating branch of the Eastern Alboran Gyre
552 (Lanoix, 1974; Viúdez and Tintoré, 1995; Fig. 10), and that mixing between surface and intermediate water masses
553 is documented to occur down to ca. 300 m water depth (Heburn and La Violette, 1990), it is conceivable that the
554 corals living currently at 327 m depth were bathed by, or situated at the limit of mixing between surface and
555 intermediate water masses during interglacial periods. Wang et al. (2019) suggest that the same phenomenon
556 occurred during the Bølling–Allerød interstadial and the Early Holocene. Higher input of MAW into the Alboran Sea
557 would lead to an increased contribution of surface waters to intermediate water masses (ShW, Fig. 2 and 10) and a
558 deepening of the pycnocline. This would promote the formation of internal waves and increase turbulence at the
559 seafloor of BRI, as suggested by the slightly higher $\overline{SS}$ values during interglacials (Fig. 5), and would have favoured
560 coral proliferation by increasing lateral nutrient supply (Fig. 10). The slight offset between planktonic and benthic
561 $\delta^{13}C$ records towards the end of MIS 7 and MIS 5 (Fig. 5) indicate that water masses were becoming more stratified
562 towards the end of interglacials and that the contribution of MAW to intermediate water masses was hence possibly
563 decreasing. Maximum *Bulimina* spp. abundance, minimum *G. subglobosa* abundance, and decreasing benthic
564 foraminiferal diversity may suggest that reduced mixing, in concomitance with important fluvial discharge (section
565 5.1.1) led to oxygen depletion at the seafloor at the transition between interglacial and glacial periods. Severe oxygen
566 depletion may explain the decline of corals at the transition from interglacial to glacial periods.

567 **5.1.3 Variability of cold-water coral mound formation between interglacial periods**

568 Highest coral content is reached during MIS 5 and corresponds to a maximum in Buliminid abundance. The Al-
569 normalized elemental ratios suggest that terrestrial input was stable during MIS 5 (Fig. 5). These stable conditions
570 would have favoured a long-lasting coral proliferation dominated by the scleractinian *D. pertusum* (Fig. 3). Marine
571 Isotope Stage 9 and 7 are also dominated by *D. pertusum.* Although MIS 7 is poorly constrained, Al-normalized
572 elemental ratios would indicate that this time period was more unstable than the previous interglacial period (Fig. 5).
573 The late Holocene is marked by a decrease in coral abundance and a dominance of *M. oculata* over *D. pertusum*. The
574 coral fragment at the top of core MD13-3462G has an age of 6.3 ka. Fink et al. (2013) obtained ages from surface
575 coral fragments at BRI that were generally between 2.7 and 3.1 ka, whilst Stalder et al. (2015) reported an age of 5.4
576 ka for a surface coral fragment sampled at BRI. Similar ages of between 3.5 and 5.8 ka were obtained on surface
577 coral fragments at the Western Melilla Coral Province (Wang et al. 2019). Dominance of the coral *M. oculata* during
578 the Late Holocene was also observed at BRI by Stalder et al. (2015), whilst Wienberg (2019) reported that *M.*
579 *oculata* already became the dominant coral species during the mid-Holocene. Previous observations suggest that *M.*
580 *oculata* is more tolerant to environmental stress than *D. pertusum* (e.g., Wienberg et al., 2009; Stalder et al., 2015).
581 Thus, the dominance of *M. oculata* at the top of the core would indicate that conditions during the late Holocene
582 were becoming increasingly unsuitable for coral proliferation, particularly for *D. pertusum*. This is consistent with
583 modern-day seafloor observations that report a near-absence of CWCs at BRI (Hebbeln et al., 2019). These

https://doi.org/10.5194/cp-2021-162
Preprint. Discussion started: 14 January 2022

combined results point to unfavourable conditions for coral proliferation during the late Holocene, as suggested by Fink et al. (2013), Stalder et al. (2015; 2018) and Wang et al. (2019). The recent decline of CWCs at the Eastern and Western Melilla Coral

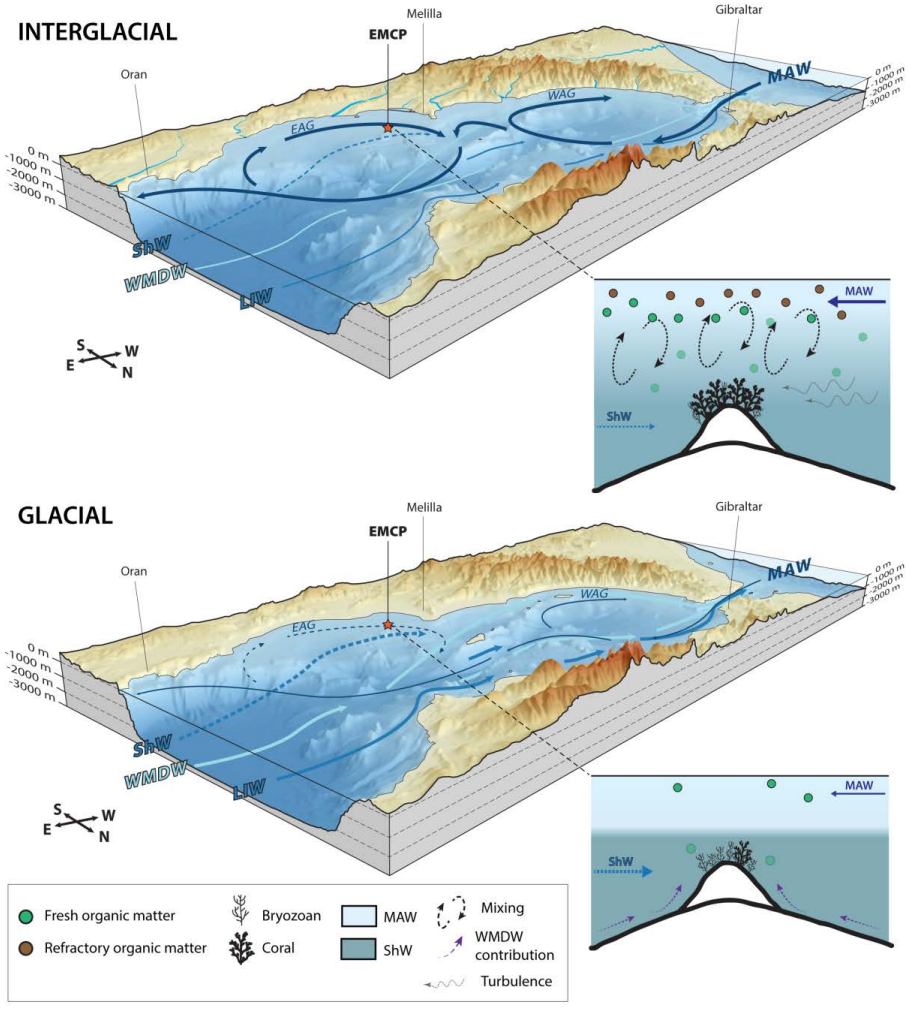

Figure 10. Three dimensional diagrams and schematic models illustrating the differences between interglacial and glacial periods and the response of the benthic community at Brittlestar Ridge I. Water masses discussed in the text are illustrated (MAW: Modified Atlantic Water, LIW: Levantine Intermediate Water, ShW: Shelf Water; WMDW: Western Mediterranean Deep Water) as well as the Western Alboran Gyre (WAG) and Eastern Alboran Gyre (EAG). The flow strength of each water mass is depicted by the thickness of the arrows. The red star indicates the location of the East Melilla Coral Province. The position of the EAG and WAG is based on observations made by Lanoix (1974), La Violette (1983), and Viúdez and Tintoré (1995). Sea level of interglacial periods corresponds to the current sea level, whilst a 100 m lower sea level stand, following observations made by

https://doi.org/10.5194/cp-2021-162
Preprint. Discussion started: 14 January 2022

Climate of the Past Discussions
Open Access
EGU

596 Rabineau et al. (2006), illustrates glacial periods. The LIW, ShW and WMDW flows follow the observations made by Ercilla et
597 al. (2016). They have been simplified and thus do not represent their exact dynamics. The schematic models are not to scale,
598 although relative depth limits between MAW and LIW have been respected. GEBCO_2019 gridded bathymetric data was used to
599 construct the diagrams.
600
601 Provinces may be linked to the establishment of more arid conditions over North Africa ca. 4 ka ago (Gasse, 2000
602 and references therein; Shanahan et al., 2015). The fluctuations in coral and bryozoan abundances between the
603 different interglacial periods may be caused by the influence of alternating dry and humid conditions.

604 **5.2 Environmental conditions during glacial periods**

605 **5.2.1 Arid continental conditions and reduced bottom currents**

606 At the exception of MIS 8, for which the boundaries are poorly defined, glacial periods are marked by a change in
607 macrofaunal composition with lower coral and higher bryozoan content in comparison to interglacial periods. Higher
608 bryozoan content during glacials at BRI is in tune with observations made at the Great Australian Bight, where lower
609 temperatures, lower sea level stand, and increased upwelling probably promoted bryozoan proliferation during
610 glacial periods (James et al., 2000; Holbourn et al., 2002). Conversely, higher temperatures and downwelling during
611 interglacials halted bryozoan extension at the Great Australian Bight (James et al., 2000; Holbourn et al., 2002).
612 Rigid erect branching bryozoans such as *B. dichotoma* are known to be fragile, and hence to prefer low energy
613 environments, being unable to withstand strong bottom currents and turbulence (Scholz and Hillmer, 1995; Bjerager
614 and Surlyk, 2007). Eutrophic environments dominated by infaunal benthic foraminifera (e.g. *Bulimina* spp.) are
615 unfavourable for erect bryozoans, the high concentration of suspended food particles clogging up their feeding
616 apparatus (Holbourn et al., 2002). Low $\overline{SS}$ values and reduced TOC content in the sediment confirm that glacial
617 periods were marked by weak bottom current velocities and organic matter flux (Fig. 5). The presence of
618 brachiopod/bivalve layers dominated by the brachiopod *Gryphus vitreus* also characterizes the glacial macrofauna
619 (Fig. 3). This species is found between 160 and 250 m depth along the Mediterranean continental margin and thrives
620 in areas dominated by moderate bottom currents (Emig and Arnaud, 1988). Thus, this species' co-occurrence with
621 bryozoans confirms that variations in sea level stand, hydrodynamics and trophic conditions govern the change in
622 macrofaunal dominance at BRI. Low organic matter flux during glacial periods has been related to predominantly
623 arid conditions over North Africa, in association with a weak North African monsoon (Gasse, 2000; Sierro et al.,
624 2005). Such arid conditions led to the complete or severe desiccation of major African lakes during the last glacial,
625 such as Lake Victoria (Talbot and Livingstone, 1989; Johnson, 1996).
626
627 The reduced precipitation and retreat of vegetation would have led to a dwindling of terrestrial input during the last
628 glacial period at BRI, as evidenced by generally lower Si/Al elemental ratio (Fig. 5). Glacial benthic foraminiferal
629 assemblages are characterized by the dominance of large epibenthic suspension feeding foraminifera, such as *L.*
630 *lobatula* and *D. coronata*, together with the infaunal *C. laevigata* (Fig. 9). This follows observations made by Stalder
631 et al. (2018) who noticed increased abundances of *Cibicides* spp., *D. coronata* and *C. laevigata* during glacial

https://doi.org/10.5194/cp-2021-162
Preprint. Discussion started: 14 January 2022


Climate of the Past Discussions

periods at BRI. These species share a preference for high quality fresh marine organic matter (De Rijk et al., 2000; Milker et al., 2009, Stalder et al., 2018). *Lobatula lobatula* and *D. coronata* prefer oxygen-rich bottom waters (Linke and Lutze; 1993; Margreth et al., 2009), whilst following Milker et al. (2009), high abundances of *C. laevigata* could be related to the presence of fine-grained material in the western Mediterranean. In the Arctic basins and Norwegian-Greenland Sea, the dominance of the epibenthic *Cibicides wuellerstorfi* (a relative of *L. lobatula*) reflects a relative low flux of organic matter (Linke and Lutze; 1993). This species tolerates vertical flux rates <2 $g.cm^{-2}.yr^{-1}$ (Altenbach, 1989). The dominance of *L. lobatula*, *D. coronata*, *C. laevigata* and Miliolids would thus indicate that the seafloor during glacial periods received less but higher quality organic matter and became more oxygenated in response to the stronger influence of intermediate and deep-water masses (Fig. 10). These observations suggest that more arid conditions during glacial periods led to a reduced influence of terrestrial input on benthic communities (Fig. 10). We propose that weaker but comparatively fresher organic matter input favoured the development of the bryozoan *B. dichotoma*. This assumption is supported by experimental observations demonstrating how erect bryozoans feed essentially on diatoms and that suspension feeding foraminifera use the same food sources (Winston, 1977; 1981; Best and Thorpe, 1994; Goldstein, 1999). Lower nutrient input appears in contrast to have been detrimental for coral proliferation but would not have led to their complete disappearance (Fig. 5 and 10). It can be hypothesized that there may exist a threshold in the quality and quantity of organic matter determining which of *D. pertusum* or *B. dichotoma* dominates the benthic environment at BRI.

5.2.2 Increased stratification and deep water overturning

As highlighted previously, the dominant macrofauna and low $\overline{SS}$ values (Fig. 3 and 5) during glacial intervals at BRI indicate weaker bottom currents. Wang et al. (2019) relate low off mound $\overline{GS}$ and high benthic foraminiferal $\delta^{13}C$ values at BRI during glacials to a dominant influence of MAW coinciding with a low sea level stand. However, whilst the benthic foraminiferal $\delta^{13}C$ values from core MD13-3462G are indeed relatively high during glacial periods, the planktonic foraminiferal $\delta^{13}C$ values do not follow the same trend (Fig. 5). The decoupling between the planktonic and benthic $\delta^{13}C$ records during the two last glacial periods, noticeably during MIS 4, suggests that water mass stratification was greater than during interglacial periods and that the seafloor was not under the direct influence of surface MAW. During glacial periods, the flow of MAW was reduced due to lower sea level and the reduced evaporation over the Mediterranean (Sierro et al., 2005). This would have reduced the contribution of MAW to ShW and weakened Western and Eastern Alboran Gyres, which would have in turn led to less mixing between surface and intermediate water masses, whilst conversely increasing stratification (Fig. 10).

Modern observations show that recently formed dense waters do not necessarily reach the deep western Mediterranean but may, in contrast, be located at intermediate water depths, above 1500 m depth (Sparnocchia et al., 1995; Millot, 1999; Ercilla et al., 2016). Ercilla et al. (2016) further exposed that WMDW can be identified at depths shallower than 500 m depth along the Moroccan margin and that it contributes to the overlying ShW, whilst deep water overturning and ventilation peaked during MIS 2 (Cacho et al., 2006; Toucanne et al., 2012). Increased oxygenation of the seafloor, as evidenced by the benthic foraminiferal assemblage (Fig. 9), may suggest that the

https://doi.org/10.5194/cp-2021-162
Preprint. Discussion started: 14 January 2022


Climate of the Past Discussions

668 contribution of well-ventilated deep and intermediate water masses at BRI was more important during glacials than
669 during interglacials (Fig. 10). The physical shape of BRI possibly plays a role in the shoaling of deep waters during
670 glacial periods. In addition, the heavier benthic C-isotope record and the abundance of fresh organic matter feeding
671 foraminifera (*L. lobatula* and *D. coronata*) during glacial periods could indicate that these waters were also nutrient-
672 rich. Although stratification between surface and intermediate water masses was greater during glacials, the stronger
673 flow of well-ventilated WMDW at BRI would explain the higher oxygen availability at the seafloor. Overall during
674 glacial periods, and in particular during the LGM, enhanced contribution of food-rich and well-ventilated WDMW to
675 overlying ShW, coupled to reduced terrestrial input and turbulence, would have promoted bryozoan proliferation
676 (Fig. 10).

677 **5.2.3 Fluctuating environmental conditions during the last glacial period**

678 The benthic and planktonic foraminifera $\delta^{18}O$ and $\delta^{13}C$ values indicate that environmental conditions were
679 particularly unstable during the last glacial period, as suggested by previous studies (Cacho et al., 2000; Martrat et
680 al., 2004; Pérez-Folgado et al., 2004; Cacho et al., 2006; Bout-Roumazeilles et al., 2007). The last glacial shows a
681 strong variability in macrofaunal and benthic foraminiferal assemblages. Maximum coral content is reached during
682 MIS 3 (Fig. 3). This increased coral content is associated to higher numbers of *G. subglobosa* and *C. laevigata*,
683 together with phases of higher Rb/Al elemental ratios (Fig. 5 and 9). These observations suggest that corals and the
684 benthic foraminiferal community positively responded to short phases of increased surface productivity related to
685 important continental runoff during MIS 3, as indicated by the high coral aggradation rates (Fig. 4B). This is
686 supported by observations made by Rogerson et al. (2018), who documented more humid conditions during MIS 3 in
687 comparison to the more arid MIS 4 and 2. Humid conditions would hence have promoted coral proliferation through
688 increased fluvial input at BRI, in the same way as during interglacial periods (section 6.1). Nevertheless, the
689 dominance of *G. subglobosa* coupled to the absence of *Bulimina* spp. and *U. mediterranea* suggests that conditions
690 were less eutrophic than during peak interglacial periods and that the organic matter reaching the seafloor may have
691 been less degraded.
692

693 **5.3 Differences between Southeast Alboran and North Atlantic coral mound formation**

694 **5.3.1 Coral proliferation and environmental forcing**

695 In the Northeast and Northwest Atlantic, corals thrive during interglacial periods whilst their proliferation is halted
696 during glacial periods (Dorschel et al., 2005; Rüggeberg et al., 2007; Frank et al., 2009; 2011; Matos et al., 2015;
697 2017). Coral proliferation at BRI does not follow the same pattern. Indeed corals develop during both interglacial
698 and glacial periods (Fig. 3). The positive response of corals to increased bottom current velocity is important in both
699 the North Atlantic and Southeast Alboran Sea. This follows the consensus that strong bottom currents are decisive
700 for the development of corals (e.g. White et al., 2005; Mienis et al., 2007; Roberts et al., 2009). The topography of
701 Brittlestar Ridge I may favour the formation of Taylor columns and the retention of organic matter, such as observed

https://doi.org/10.5194/cp-2021-162
Preprint. Discussion started: 14 January 2022

Climate of the Past Discussions
Open Access
EGU

in the Rockall Trough (Northeast Atlantic, White, 2007). However, benthic foraminiferal assemblages associated to phases of coral proliferation in the Northeast Atlantic (Rüggeberg et al., 2007) and in the Southeast Alboran Sea (this study) differ. Benthic foraminiferal assemblages associated to phases of sustained coral proliferation at Propeller Mound (Northeast Atlantic) are essentially characterized by large epibenthic foraminifera (*L. lobatula*, *Cibicides refulgens*, *D. coronata*, and *Planulina ariminensis*) and the infaunal *Trifarina bradyi* (Rüggeberg et al., 2007). In contrast, at BRI, higher abundances of *L. lobatula*, *D. coronata* and *T. angulosa* are associated to glacial periods or transition phases between interglacial and glacial periods with low coral abundance, while small infaunal foraminifera dominate phases of coral proliferation (Fig. 9). These contrasting observations suggest differences in food supply and bottom current regimes. Corals in the Northeast Atlantic thrive on fresh marine-derived organic matter resulting from North Atlantic blooms which are fuelled by upwelling (Dickinson et al., 1980). In contrast, corals at BRI are likely supplied by plankton blooms triggered by the input of degraded fluvial organic matter during interglacial times, whilst aeolian dust input allows corals to survive during glacial times by triggering local moderate nutrient supply to the seafloor. In this regard, coral mounds situated in the Southeast Alboran Sea show more similarities to mounds located in the Viosca Knoll area, where the dispersal of terrestrial organic matter by the Mississippi River triggers an increase in primary productivity, providing nutrients for coral communities during interglacial periods (Mienis et al., 2012). The respective shallow location and proximity of BRI to the continent explains the higher influence of continental runoff on coral communities than in the deeper Northeast Atlantic sites. As such, water mass rearrangements appear to be of secondary importance, whilst the input of terrestrial organic matter would be the primary factor triggering coral proliferation at BRI.

5.3.2 Long-term coral mound build-up

Long-term coral mound formation at BRI and in the Porcupine Seabight do not show the same temporal distribution. Indeed, mound aggradation in the Porcupine Seabight is restricted to interglacial periods, whilst winnowing and mass wasting are considered as precursor events for the re-initiation of coral proliferation during glacial terminations (Rüggeberg et al., 2007; Frank et al., 2011). In contrast, benthic foraminiferal assemblages and $\overline{SS}$ would indicate that terminations were not marked by winnowing or erosional events at BRI (Fig. 5 and 9). Thus, the environmental mechanisms triggering the reset of coral proliferation at the onset of interglacials at BRI appear to be different from the Northeast Atlantic. Long-term coral mound formation at BRI took place during interglacial and glacial periods, though at much lower aggradation rates than in the Porcupine Seabight (Fig. 4B; Frank et al., 2011). Highest aggradation rates occur during MIS 3 and MIS 6. The maximum rate of ca. 10 cm.ky^{-1} is reached during the middle of MIS 3 with a short peak to 18 cm.ky^{-1}, whilst rates do not exceed ca. 4 cm.ky^{-1} during interglacial periods (Fig. 4B).

The limited coral mound build-up during both interglacial and glacial periods at BRI can explain the observed $\delta^{18}O$ values throughout core MD13-2462G which demonstrate typical interglacial/glacial variations (Fig. 4, Cacho et al., 1999; Lisiecki and Raymo, 2005; Cacho et al., 2006). The $\delta^{18}O$ values recorded for interglacial and glacial periods

https://doi.org/10.5194/cp-2021-162
Preprint. Discussion started: 14 January 2022

are a clear indication that coral mounds at BRI demonstrate a more continuous build-up history across interglacial/glacial periods than their North Atlantic counterparts. Mound aggradation rates in core MD13-3462G are comparable to inactive or abandoned reefs in the Porcupine Seabight, i.e. <5 cm.ky^{-1} (Frank et al., 2011), thus suggesting that CWCs did not thrive at the site of core MD13-3462G but rather developed under stressful environmental conditions. Average long-term mound aggradation rates at BRI show more similarities with mounds situated along the Mauritanian margin that developed during the last glacial (28-45 cm.ky^{-1}) but also during the last interglacial period (16 cm.ky^{-1}; Wienberg et al., 2018; Wienberg and Titschak, 2015). In contrast with Atlantic CWC mounds, mounds from the East Melilla Coral Province show a high contribution of the erect cheleistome bryozoan *B. dichotoma*. Based on mound aggradation rates and macrofaunal content, we propose that *B. dichotoma* communities favoured mound formation at BRI, noticeably during glacial periods, by capturing fine-grained sediments in a similar way as CWCs do (Fig. 3 and 8). As such, mounds at BRI stand out and may be considered as mixed *B. dichotoma*/CWC mounds, rather than CWC mounds per se.

Conclusions

The multiproxy study of core MD13-3462G provides information on the long-term build-up of a cold-water coral mound at Brittlestar Ridge I. Two important points can be highlighted:

(1) Cold-water coral mound build-up takes place during both interglacial and glacial periods. Average coral mound aggradation rates are particularly low, varying between 1 and 10 cm.ky^{-1}. Low mound aggradation rates during interglacial and glacial periods suggest that corals did not thrive but rather developed under stressful environmental conditions at Brittlestar Ridge I. During interglacial periods, coral development is driven by the combination of increased terrestrial input and enhanced turbulence at the seafloor. The dominant influence of warm and moist Atlantic air masses together with intensified Western and Eastern Alboran Gyres promoted high food availability at the seafloor during interglacial periods. In contrast, more arid continental conditions and the upwelling of deep-water masses would have characterized glacial conditions. The bryozoan *Buskea dichotoma* appears to be better suited to these glacial environmental conditions than the scleractinian *D. pertusum*. Overall, our results demonstrate the paramount importance of enhanced terrestrial input as a trigger for cold-water coral mound build-up in the Southeast Alboran Sea.

(2) The planktonic and benthic $\delta^{18}O$ record of cold-water coral mound sediments at Brittlestar Ridge I shows typical interglacial/glacial variations. This is in contrast with $\delta^{18}O$ records observed in sediments from Northeast Atlantic cold-water coral mounds and underlines the discrepancies in mound build-up processes between the two regions.

From a wider perspective, the build-up of cold-water coral mounds situated at Brittlestar Ridge I during both interglacial and glacial periods stresses how cold-water coral communities are capable of withstanding important

https://doi.org/10.5194/cp-2021-162
Preprint. Discussion started: 14 January 2022

772 environmental changes and to survive and adapt to different climatic conditions. This study further suggests that the
773 role of associated species, such as rigid erect bryozoans, may be associated to the resilience of coral ecosystems.

774 **Data availability**

775 The datasets used in this study are available at the open-access repository PANGEA:
776 https://doi.pangaea.de/10.1594/PANGAEA.915601.

777 **Sample availability**

778 Archive halves of all core sections investigated for this study are available at the Department of Geosciences,
779 University of Fribourg (Switzerland). The sediment residues and the splits of each sample analysed for benthic
780 foraminiferal assemblages are stored at the Department of Geosciences, University of Fribourg (Switzerland).
781 Bryozoans identified in this study are available at the Palaeontological Museum of the University of Catania (Italy).

782 **Author contributions**

783 RF: writing (original draft), visualization, conceptualization, core sampling, investigation (benthic foraminiferal
784 assemblages, main macrofaunal fragments, particle size analysis, stable isotope measurements assisted by TV and
785 radiocarbon dating assisted by IH). EF: conceptualization, writing (review and editing), XRF investigation (assisted
786 by HV), preparation of samples for Uranium-series dating and RockEval6 pyrolysis. ARü: conceptualization, writing
787 (review and editing), supervision. EH: investigation (CT analysis, macrofaunal quantification). VR: writing (review
788 and editing), visualization. TV: writing (review and editing), investigation (stable isotope measurements), resources.
789 IH: writing (review and editing), investigation (radiocarbon dating), resources. ARo: writing (review and editing),
790 investigation (bryozoan taxonomy). DVR: writing (review and editing), resources. TA: writing (review and editing),
791 investigation (RockEval6 pyrolysis), resources. HV: writing (review and editing), investigation (XRF), resources. NF
792 & TK: writing (review and editing), investigation (Uranium-series dating). AF: investigation (core description, CT
793 data analysis, XRF data analysis), conceptualization, writing (review and editing), project administration, funding
794 acquisition, supervision.

795 **Conflict of interests**

796 The authors declare that they have no conflict of interest.

https://doi.org/10.5194/cp-2021-162
Preprint. Discussion started: 14 January 2022

Climate of the Past Discussions

Acknowledgements

We thank the SNSF (Swiss National Science Foundation) projects 'Unconventional Carbonate Factories' and '4D-Diagenesis@Mound' (project numbers 200020_153125 and 200021_149247) for funding this research. We also are grateful for the ship time provided by IPEV on the R/V *Marion Dufresne II* within the framework of the EuroFLEETS GATEWAYS project (grant agreement 228344). We further thank Tim Collart for the help he provided with the *Rysgran* package for R and Marc Schori for his help with the *ArcGIS* software. We further acknowledge the help of Rene Eichstädter and Andrea Schröder-Ritzrau regarding Uranium-series dating and quality control. The DFG has provided funding for the Uranium-series dating of corals via the project FR1341/9-1.

References

Addamo, A.M., Vertino, A., Stolarski, J., García-Jiménez, R., Taviani, M., and Machordom, A.: Merging scleractinian genera: the overwhelming genetic similarity between solitary *Desmophyllum* and colonial *Lophelia*, BMC Evol Biol, 16, 108, 2016.

Altenbach, A.V. and Sarnthein, M.: Productivity Record in Benthic Foraminifera, in: Productivity of the Ocean: Present and Past, edited by: Berger, W.H., Smetacek, V.S., and Wefer, G., John Wiley & Sons Limited, 255-269, 1989.

Best, M.A. and Thorpe, J.P.: Particle size, clearance rate and feeding efficiency in marine Bryozoa, in: Biology and Palaeobiology of Bryozoans, edited by: Hayward, P.J., Ryland, J.S., and Taylor, P.D., Olsen and Olsen, Fredensborg, Denmark, 9-14, 1994.

Beuck, L. and Freiwald, A.: Bioerosion patterns in a deep-water *Lophelia pertusa* (Scleractinia) thicket (Propeller Mound, northern Porcupine Seabight), in: Cold-water corals and ecosystems, published by: Freiwald, A. and Roberts, J.M., Springer-Verlag, Berlin Heidelberg, 915-936, 2005.

Bjerager, M. and Surlyk, F.: Benthic palaeoecology of Danian deep-shelf bryozoan mounds in the Danish Basin, Palaeogeogr Palaeocl, 250, 184-215, 2007.

Bout-Roumazeilles, V., Combourieu Nebout, N., Peyron, O., Cortijo, E., Landais, A., and Masson-Delmotte, V.: Connection between South Mediterranean climate and North African atmospheric circulation during the last 50,000 yr BP North Atlantic cold events, Quaternary Sci Rev, 26, 3197-3215, 2007.

Braun, K., Nehme, C., Pickering, R., Rogerson, M., and Scroxton, N.: A window into Africa's past hydoclimates: the SISAL_V1 database contribution, Quaternary, 2, 4, 2019.

Bromley, R.G.: Preliminary study of bioerosion in the deep-water coral *Lophelia*, Pleistocene, Rhodes, Greece, in: Cold-water Corals and Ecosystems, edited by: Freiwald, A. and Roberts, J.M., Springer-Verlag, Berlin Heidelberg, 895-914, 2005.

Cacho, I., Grimalt, J.O., Pelejero, C., Canals, M., Sierro, F.J., Flores, J.A., and Shackleton, N.: Dansgaard-Oeschger and Heinrich event imprints in Alboran Sea paleotemperatures, Paleoceanography, 14, 698-705, 1999.

Cacho, I., Grimalt, J.O., Sierro, F.J., Scackleton, N.J., and Canals, M.: Evidence for enhanced Mediterranean thermohaline circulation during rapid climatic coolings, Earth Planet Sc Lett, 183, 417-429, 2000.

https://doi.org/10.5194/cp-2021-162
Preprint. Discussion started: 14 January 2022

832 Cacho, I., Shackleton, N., Elderfield, H., Sierro, F.J., and Grimalt, J.O.: Glacial rapid variability in deep-water
833 temperature and $\delta^{18}O$ from the Western Mediterranean Sea, Quaternary Sci Rev, 25, 3294-3311, 2006.
834 Calvert, S.E. and Pedersen, T.F.: Elemental Proxies for Palaeoclimatic and Palaeoceanographic Variability in Marine
835 Sediments: Interpretation and Application, in: Developments in Marine Geology, edited by Hillaire–Marcel, C.
836 and De Vernal, A., Elsevier, 2007
837 Caquineau, S., Gaudichet, A., Gomes, L., and Legrand, M.: Mineralogy of Saharan dust transported over
838 northwestern tropical Atlantic Ocean in relation to source regions, J Geophys Res-Atmos, 107, 1-14, 2002.
839 Caquineau, S., Gaudichet, A., Gomes, L., Magonthier, M-C., Chatenet, B.: Saharan dust: Clay ratio as a relevant
840 tracer to assess the origin of soil-derived aerosols. Geophysical Research Letters, 25, 983-986, 1998.
841 Carlier, A., Le Guilloux, E., Olu, K., Sarrazin, J., Mastrototaro, F., Taviani, M., and Clavier, J.: Trophic relationships
842 in a deep Mediterranean cold-water coral bank (Santa Maria di Leuca, Ionian Sea). Mar Ecol Prog Ser, 397,
843 125-137, 2009.
844 Cheng, H., Adkins, J., Lawrence Edwards, R., and Boyle, E.A.: U-Th dating of deep-sea corals, Geochim
845 Cosmochim Ac, 64, 14, 2401-2416, 2000.
846 Clarke, K.R. and Gorley, R.N.: PRIMER v6: User Manual/Tutorial (Plymouth Routines in Multivariate Ecological
847 Research), PRIMER-E, Plymouth, 2006.
848 Comas, M., and Pinheiro, L.M.: The Melilla carbonate mounds: do deep-water coral mounds count on seeping fluids
849 in the Alboran Sea? Rapp. Comm. Int. Mer Médit, 39, 16, 2010.
850 Comas, M.C., Pinheiro, L.M., Ivanov, M. and TTR-17 Leg 1 Scientific Party: Deep-water coral mounds in the
851 Alboran Sea: the Melilla mounds field revisited, IOC Workshop Report No. 220, Granada (Spain), 2-5 February
852 2009, 2009.
853 Comas, M.C., Platt, J.P., Soto, J.I. and Watts, A.B.: The origin and tectonic history of the Alboran Basin: insights
854 from Leg 161 results, Proceedings of the Ocean Drilling Program 161, Scientific Results, 1999.
855 Corbera, C., Lo Iacono, C., Standish, D., Anagnostou, E., Titschack, J., Katsamenis, O., Cacho, I., Van Rooij, D.,
856 Huvenne, V.A.I., and Foster, G.L.: Glacio-eustatic variations and sapropel events as main controls on the Middle
857 Pleistocene-Holocene evolution of the Cabliers Coral Mound Province (W Mediterranean). Quaternary Science
858 Reviews, 253, 106783, 2021.
859 Coulthard, T.J., Ramirez, J.A., Barton, N., Rogerson, M., and Brucher, T.: Were rivers flowing across the Sahara
860 during the last interglacial? Implications for human migration through Africa, PLoS One, 8, e74834. 2013.
861 Croudace, I.W., Rothwell, R.G.: Micro-XRF Studies of Sediment Cores: Applications of a non-destructive tool for
862 the environmental sciences. Developments in Paleoenvironmental Research (Springer), 17, 656 pp, 2015.
863 Davies, A.J. and Guinotte, J.M.: Global habitat suitability for framework-forming cold-water corals, PLoS One 6,
864 e18483, 2011.
865 Davies, A.J., Duineveld, G., Lavaleye, M., Bergman, M., van Haren, H., and Roberts, J.: Downwelling and deep-
866 water bottom currents as food supply mechanisms to the cold-water coral *Lophelia pertusa* (*Scleractinia*) at the
867 Mingulay Reef Complex, Limnol Oceanogr, 54, 620-629, 2009.

https://doi.org/10.5194/cp-2021-162
Preprint. Discussion started: 14 January 2022

868 De Mol, B., Van Rensbergen, P., Pillen, S., Van Herreweghe, K., Van Rooij, D., McDonnell, A., Huvenne, V.A.I.,
869 Ivanov, M., Swennen, R., and Henriet, J.-P.: Large deep-water coral banks in the Porcupine Basin, southwest of
870 Ireland, Mar Geol, 188, 193-231, 2002.
871 De Rijk, S., Jorissen, F., Rohling, E.J., and Troelstra, S.R.: Organic flux control on bathymetric zonation of
872 Mediterranean benthic foraminifera, Mar Micropaleontol, 40, 151-166, 2000.
873 Dessandier, P.-A., Bonnin, J., Kim, J.-H., Bichon, S., Deflandre, B., Grémare, A., and Sinninghe Damsté, J.S.:
874 Impact of organic matter source and quality on living benthic foraminiferal distribution on a river-dominated
875 continental margin: A study of the Portuguese margin, J. Geophys. Res. Biogeosci., 121,1689-1714, 2016.
876 Dickinson, R.R., Gurbutt, P.A., and Pillai, V.N.: Satellite evidence of enhanced upwelling along the European
877 continental slope, Geology, 813-819, 1980.
878 Do Couto, D., Gorini, C., Jolivet, L., Lebret, N., Augier, R., Gumiaux, C., d'Acremont, E., Ammar, A., Jabour, H.,
879 and Auxietre, J.-L.: Tectonic and stratigraphic evolution of the Western Alboran Sea Basin in the last 25 Myrs,
880 Tectonophysics, 677-678, 280-311, 2016.
881 Dorschel, B., Hebbeln, D., Foubert, A., White, M., and Wheeler, A.J.: Hydrodynamics and cold-water coral facies
882 distribution related to recent sedimentary processes at Galway Mound west of Ireland, Mar Geol, 244, 184-195,
883 2007.
884 Dorschel, B., Hebbeln, D., Ruggeberg, A., Dullo, W-C, and Freiwald, A.: Growth and erosion of a cold-water coral
885 covered carbonate mound in the Northeast Atlantic during the Late Pleistocene and Holocene, Earth Planet Sc
886 Lett, 233, 33-44, 2005.
887 Drinia, H. and Dermitzakis, M.D.: The response of benthic foraminifera to palaeoenvironmental disturbance: A
888 quantitative approach in turbidite-like successions, N. Jb. Geol. Paläont. Abh, 258, 3, 325–338, 2010.
889 Duggen, S., Hoernle, K., Klügel, A., Geldmacher, J., Thirlwall, M., Hauff, F., Lowry, D., and Oates, N.:
890 Geochemical zonation of the Miocene Alborán Basin volcanism (westernmost Mediterranean): geodynamic
891 implications, Contrib Mineral Petr, 156, 577-593, 2008.
892 Dullo W-C., Flögel, S. and Rüggeberg, A.: Cold-water coral growth in relation to the hydrography of the Celtic and
893 Nordic European continental margin, Mar Ecol Prog Ser, 371, 165-176, 2008.
894 Eisele, M., Frank, N., Wienberg, C., Hebbeln, D., López Correa, M., Douville, E., and Freiwald, A.: Productivity
895 controlled cold-water coral growth periods during the last glacial off Mauritania, Mar Geol, 280, 143-149, 2011.
896 Eisele, M., Hebbeln, D., and Wienberg, C.: Growth history of a cold-water coral covered carbonate mound —
897 Galway Mound, Porcupine Seabight, NE-Atlantic, Mar Geol, 253, 160-169, 2008.
898 Emelyanov, E.M. and Shimkus, K.M.: Geochemistry and sedimentology of the Mediterranean Sea, Springer Science
899 and Business Media, 2012.
900 Emig, C.C. and Arnaud, P.M.: Observations en submersible sur la densité des populations de *Gryphus vitreus*
901 (Brachiopode) le long de la marge continentale de Provence (Méditerranée nord-occidentale), C. R. Acad. Sci.
902 Paris, 306, 501-505, 1988.
903 Ercilla, G., Juan, C., Hernández-Molina, J., Bruno, M., Estrada, F., Alonso, B., Casas, D., Farran, M., Llave, E.,
904 García, Vázquez, J.T., D'Acremont, E., Gorini, C., Palomino, D., Valencia, J., El Moumni, B., and Ammar, A.:

https://doi.org/10.5194/cp-2021-162
Preprint. Discussion started: 14 January 2022

Significance of bottom currents in deep-sea morphodynamics: An example from the Alboran Sea, Mar Geol, 378, 157-170, 2016.

Espitalié, J., Deroo, G., and Marquis, F.: La Pyrolyse Rock-Eval et ses applications, Revue de l'Institut Français du Pétrole, 40, 5, 1-34, 1986.

Faccenna, C., Piromallo, C., Crespo-Blanc, A., Jolivet, L., and Rossetti, F.: Lateral slab deformation and the origin of the western Mediterranean arcs, Tectonics, 23, 2004.

Fantasia, A., Adatte, T., Spangenberg, J.E., Font, E., Duarte, L.V., and Föllmi, K.B.: Global versus local processes during the Pliensbachian-Toarcian transition at the Peniche GSSP, Portugal: a multi-proxy record, Earth-Sci Rev, 198, 102932, 2019.

Fariduddin, M. and Loubere, P.: The surface ocean productivity response of deeper water benthic foraminifera in the Atlantic Ocean, Mar Micropaleontol, 32, 289-310, 1997.

Fentimen, R., Feenstra, E., Rüggeberg, A., Vennemann, T., Hajdas, I., Adatte, T., Van Rooij, D., and Foubert, A.: Cold-Water Coral Mound Archive Provides Unique Insights Into Intermediate Water Mass Dynamics in the Alboran Sea During the Last Deglaciation, Frontiers in Marine Science, 7, 354, 2020a.

Fentimen, R., Lim, A., Rüggeberg, A., Wheeler, A.J., Van Rooij, D., and Foubert, A.: Impact of bottom water currents on benthic foraminiferal assemblages in a cold-water coral environment: The Moira Mounds (NE Atlantic), Mar. Micropaleontol, 154, 101799, 2020b.

Fink, H.G., Wienberg, C., De Pol-Holz, R., and Hebbeln, D.: Spatio-temporal distribution patterns of Mediterranean cold-water corals (*Lophelia pertusa* and *Madrepora oculata*) during the past 14,000 years, Deep-Sea Res Pt I, 103, 37-48, 2015.

Fink, H.G., Wienberg, C., De Pol-Holz, R., Wintersteller, P., and Hebbeln, D.: Cold-water coral growth in the Alboran Sea related to high productivity during the Late Pleistocene and Holocene, Mar Geol, 339, 71-82, 2013.

Folk, R.L. and Ward, W.C.: A Study in the Significance of Grain-Size Parameters, J Sediment Petrol, 27, 3-26, 1957.

Fontanier, C., Jorissen, F.J., Chaillou, G., David, C., Anschutz, P., and Lafon, V.: Seasonal and interannual variability of benthic foraminiferal faunas at 550m depth in the Bay of Biscay, Deep-Sea Res Pt I, 50, 457-494, 2003.

Fontanier, C., Jorissen, F.J., Licari, L., Alexandre, A., Anschutz, P., and Carbonel, P.: Live benthic foraminiferal faunas from the Bay of Biscay: faunal density, composition, and microhabitats, Deep-Sea Res Pt I, 49, 751-785, 2002.

Foubert, A. and Henriet, J.-P.: Nature and Significance of the Recent Carbonate Mound Record, Lecture Notes in Earth Sciences, 126, Springer-Verlag, Berlin, 298 pp., 2009.

Frank, N., Freiwald, A., Correa, M.L., Wienberg, C., Eisele, M., Hebbeln, D., Van Rooij, D., Henriet, J.P., Colin, C., van Weering, T., de Haas, H., Buhl-Mortensen, P., Roberts, J.M., De Mol, B., Douville, E., Blamart, D., and Hatte, C.: Northeastern Atlantic cold-water coral reefs and climate, Geology, 39, 743-746, 2011.

Frank, N., Paterne, M., Ayliffe, L., van Weering, T., Henriet, J.-P., and Blamart, D.: Eastern North Atlantic deep-sea corals: tracing upper intermediate water $\Delta^{14}C$ during the Holocene, Earth Planet Sc Lett, 219, 297-309, 2004.

https://doi.org/10.5194/cp-2021-162
Preprint. Discussion started: 14 January 2022

941 Frank, N., Ricard, E., Lutringer-Paquet, A., van der Land, C., Colin, C., Blamart, D., Foubert, A., Van Rooij, D.,
942 Henriet, J.-P., de Haas, H., and van Weering, T.: The Holocene occurrence of cold water corals in the NE
943 Atlantic: Implications for coral carbonate mound evolution, Mar Geol, 266, 129-142, 2009.
944 Freiwald, A., Fosså, J.H., Grehan, A., Koslow, T., and Roberts, J.M.: Cold-water coral Reefs, UNEP_WCMC,
945 Cambridge, UK, 2004.
946 Gasse, F.: Hydrological changes in the African tropics since the Last Glacial Maximum, Quaternary Sci Rev, 19,
947 189-211, 2000.
948 Gasse, F. and Roberts, C.N.: Late Quaternary hydrologic changes in the arid and semiarid belt of northern Africa, in:
949 The Hadley Circulation: Present, Past and Future, edited by: Diaz, H.F. and Bradley, R.S., Kluwer Academic
950 Publishers, 313-345, 2005.
951 Gilbert, E.R., Camargo, M.G. and Sandrini-Neto, L.: rysgran: Grain size analysis, textural classifications and
952 distribution of unconsolidated sediments, R package version 2.1.0, https://CRAN.R-
953 project.org/package=rysgran, 2015.
954 Goldstein S.T.: Foraminifera: A biological overview, in: Modern Foraminifera, edited by: Sen Gupta, B.K., 37– 55,
955 Kluwer Acad., Norwell, Mass., 1999.
956 Gooday, A.J.: The Biology of Deep-Sea Foraminifera: A Review of Some Advances and Their Applications in
957 Paleoceanography, Palaios, 9, 14-31, 1993.
958 Gregory, B.R.B., Patterson, T.R., Reinhardt, E.G., Galloway, J.M., and Roe, H.R.: An evaluation of methodologies
959 for calibrating Itrax X-ray fluorescence counts with ICP-MS concentration data for discrete sediment samples,
960 Chem Geol, 525, 12-27, 2019.
961 Guieu, C., Thomas, A.J.: Saharan Aerosols: From the Soil to the Ocean. In: Guerzoni, S., Chester, R. (Eds.) *The*
962 *Impact of Desert Dust Across the Mediterranean*. Springer Netherlands: Dordrecht, 408 pp, 1996.
963 Hanz, U., Wienberg, C., Hebbeln, D., Duineveld, G., Lavaleye, M., Juva, K., Dullo, W.-C., Freiwald, A.,
964 Tamborrino, L., Reichart, G.-J., Flögel, S., and Mienis, F.: Environmental factors influencing cold-water coral
965 ecosystems in the oxygen minimum zones on the Angolan and Namibian margins, Biogeosciences, 1-37, 2019.
966 Hebbeln, D.: Highly variable submarine landscapes in the Alborán Sea created by cold-water corals, in:
967 Mediterranean Cold-Water Corals: Past, Present and Future, published by: Orejas, C. and Jiménez, C., Springer
968 series: Coral Reefs of the World 9, Springer International Publishing, 61-65, 2019.
969 Hebbeln, D., Van Rooij, D., and Wienberg, C.: Good neighbours shaped by vigorous currents: Cold-water coral
970 mounds and contourites in the North Atlantic, Mar Geol, 378, 171-185, 2016.
971 Heburn, G.W. and La Violette, P.E.: Variations in the structure of the anticyclonic gyres found in the Alboran Sea, J
972 Geophys Res, 95, 1990.
973 Holbourn, A., Kuhnt, and W., James, N.: Late Pleistocene bryozoan reef mounds of the Great Australian Bight:
974 Isotope stratigraphy and benthic foraminiferal record, Paleoceanography, 17, 2002.
975 Huvenne, V.A.I., De Haas, H., Dekindt, K., Henriet, J-P., Kozachenko, M., Olu-Le Roy, K., and Wheeler, A.J.: The
976 seabed appearance of different coral bank provinces in the Porcupine Seabight, NE Atlantic: results from
977 sidescan sonar and ROV seabed mapping, in: Cold-water Corals and Ecosystems, edited by: Freiwald, A. and
978 Roberts, J.M., Springer-Verlag, Berlin, Heidelberg, 536-569, 2005.

https://doi.org/10.5194/cp-2021-162
Preprint. Discussion started: 14 January 2022

979 Huvenne, V.A.I., Masson, D.G., and Wheeler, A.J.: Sediment dynamics of a sandy contourite: the sedimentary
980 context of the Darwin cold-water coral mounds, Northern Rockall Trough, Int J Earth Sci98, 865-884, 2009.
981 Jaffey, A.H., Flynn, K.F., Glendenin, L.E., Bentley, W.C., and Essling, A.M.: Precision measurements of half-lives
982 and specific activities of ^{235}U and ^{238}U, Phys Rev, 4, 5, 1889-1906, 1971.
983 James, N.P., Feary, D.A., Surlyk, F., Toni Simo, J.A., Betzler, C., Holbourn, A.E., Li, Q., Matsuda, H., Machiyama,
984 H., Brooks, G.R., Andres, M.S., Hine, A.C., and Malone, M.J.: Quaternary bryozoan reef mounds in cool-water,
985 upper slope environments: Great Australian Bight, Geology, 28, 2000.
986 Johnson, T.C.: Sedimentary processes and signals of past climate change in the large lakes of East African Rift
987 Valley, in: Limnology, Climatology and Paleoclimatology of the East African Lakes, edited by: Johnson, T.C.
988 and Odada, E.O., The Gordon and Breach, Amsterdam, 367-412, 1996.
989 Jorissen, F.J.: The distribution of benthic foraminifera in the Adriatic Sea, Mar Micropaleontol, 12, 21-48, 1987.
990 Kano, A., Ferdelman, T.G., Williams, T., Henriet, J.-P., Ishikawa, T., Kawagoe, N., Takashima, C., Kakizaki, Y.,
991 Abe, K., Sakai, S., Browning, E.L., and Li, X.: Age constraints on the origin and growth history of a deep-water
992 coral mound in the northeast Atlantic drilled during Integrated Ocean Drilling Program Expedition 307,
993 Geology, 35, 2007.
994 Katz, E.J.: The Levantine Intermediate Water between the Strait of Sicily and the Strait of Gibraltar, Deep-Sea Res,
995 19, 507-520, 1972.
996 Kenyon, N.H., Akhmetzhanov, A.M., Wheeler, A.J., van Weering, T.C.E., de Haas, H., and Ivanov, M.K.: Giant
997 carbonate mud mounds in the southern Rockall Trough, Mar Geol, 195, 5-30, 2003.
998 Knippertz, P., Christoph, M., and Speth, P.: Long-term precipitation variability in Morocco and the link to the large-
999 scale circulation in recent and future climates, Meteorol Atmos Phys, 83, 67-88, 2003.
1000 Koho, K.A., García, R., de Stigter, H.C., Epping, E., Koning, E., Kouwenhoven, T.J., and van der Zwaan, G.J.:
1001 Sedimentary labile organic carbon and pore water redox control on species distribution of benthic foraminifera:
1002 A case study from Lisbon–Setúbal Canyon (southern Portugal), Prog Oceanogr, 79, 55-82, 2008.
1003 Lavaysse, C., Flamant, C., Janicot, S., Parker, D.J., Lafore, J.-P., Sultan, B., and Pelon, J.: Seasonal evolution of the
1004 West African heat low: a climatological perspective, Clim Dyn, 33, 313-330, 2009.
1005 La Violette, P.E.: The Advection of Submesoscale Thermal Features in the Alboran Sea Gyres, J Phys Oceanogr, 14,
1006 550-565, 1983.
1007 Lafuente, J.G., Camno, N., Vargas, M., Rubín, J.P., and Hernández-Guerra, A.: Evolution of the Alboran Sea
1008 hydrographic structures during July 1993, Deep-Sea Res Pt I, 45, 39-65, 1998.
1009 Lanoix, R.: Projet Alboran: étude hydrologique et dynamique de la mer d'Alboran, Technical Report 66, NATO,
1010 Brussels, Belgium, 1974.
1011 Linke, P. and Lutze, G.F.: Microhabitat preferences of benthic foraminifera—a static concept or a dynamic
1012 adaptation to optimize food acquisition?, Mar Micropaleontol, 20, 215-234, 1993.
1013 Lionello, P., Trigo, I.F., Gil, V., Liberato, M.L.R., Nissen, K.M., Pinto, J.G., Raible, C.C., Reale, M., Tanzarella, A.,
1014 Trigo, R.M., Ulbrich, S., and Ulbrich U.: Objective climatology of cyclones in the Mediterranean region: a
1015 consensus view among methods with different system identification and tracking criteria, Tellus A, 68, 1,
1016 29391, 2016.

https://doi.org/10.5194/cp-2021-162
Preprint. Discussion started: 14 January 2022

1017 Lisiecki, L.E. and Raymo, M.E.: A Pliocene-Pleistocene stack of 57 globally distributed benthic $\delta^{18}O$ records,
1018 Paleoceanography, 20, PA1003, 2005.
1019 Lo Iacono, C., Gràcia, E., Ranero, C.R., Emelianov, M., Huvenne, V.A.I., Bartolomé, R., Booth-Rea, G., Prades, J.,
1020 Ambroso, S., Dominguez, C., Grinyó, J., Rubio, E., and Torrent, J.: The West Melilla cold water coral mounds,
1021 Eastern Alboran Sea: Morphological characterization and environmental context, Deep-Sea Res Pt II, 99, 316-
1022 326, 2014.
1023 López Correa, M., Montagna, P., Joseph, N., Rüggeberg, A., Fietzke, J., Flögel, S., Dorschel, B., Goldstein, S.L.,
1024 Wheeler, A., and Freiwald, A.: Preboreal onset of cold-water coral growth beyond the Arctic Circle revealed by
1025 coupled radiocarbon and U-series dating and neodymium isotopes, Quaternary Sci Rev, 34, 24-43, 2012.
1026 Löwemark, L., Chen, H.F., Yang, T.N., Kylander, M., Yu, E.F., Hsu, Y.W., Lee, T.Q., Song, S.R., Jarvis, S.:
1027 Normalizing XRF-scanner data: A cautionary note on the interpretation of high-resolution records from organic-
1028 rich lakes. Journal of Asian Earth Sciences, 40, 1250-56, 2011.
1029 Lutze, G.F. and Coulbourn, W.T.: Recent benthic foraminifera from the continental margin of Northwest Africa:
1030 community structure and distribution, Mar Micropaleontol, 8, 361-401, 1984.
1031 Mackensen, A., Schmiedl, G., Harloff, J., and Giese, M.: Deep-sea foraminifera in the South Atlantic Ocean:
1032 Ecology and assemblage generation, Micropaleontology, 41, 342-358, 1995.
1033 Margreth, S., Rüggeberg, A., and Spezzaferri, S.: Benthic foraminifera as bioindicator for cold-water coral reef
1034 ecosystems along the Irish margin, Deep-Sea Res Pt I, 56, 2216-2234, 2009.
1035 Martinez-Ruiz, F., Kastner, M., Gallego-Torres, D., Rodrigo-Gámiz, M., Nieto-Moreno, V., Ortega-Huertas, M.:
1036 Paleoclimate and paleoceanography over the past 20,000 yr in the Mediterranean Sea Basins as indicated by
1037 sediment elemental proxies. Quaternary Science Reviews, 107, 25-46, 2015.
1038 Martrat, B., Grimalt, J.O., Lopez-Martinez, C., Cacho, I., Sierro, F.J., Flores, J.A., Zahn, R., Canals, M., Curtis, J.H.,
1039 and Hodell, D.A.: Abrupt temperature changes in the Western Mediterranean over the past 250,000 years,
1040 Science, 306, 1762-1765, 2004.
1041 Masqué, P., Fabres, J., Canals, M., Sanchez-Cabeza, J.A., Sanchez-Vidal, A., Cacho, I., Calafat, A.M., and Bruach,
1042 J.M: Accumulation rates of major constituents of hemipelagic sediments in the deep Alboran Sea: a centennial
1043 perspective of sedimentary dynamics, Mar Geol, 193, 207-33, 2003.
1044 Mastrototaro F., D'Onghia G., Corriero G., Matarrese A., Maiorano P., Panetta P., Gherardi M., Longo C., Rosso A.,
1045 Sciuto F., Sanfilippo R., Gravili C., Boero F, Taviani M., and Tursi A.: Biodiversity of the white coral bank off
1046 Cape Santa Maria di Leuca (Mediterranean Sea): An update, Deep-Sea Res Pt II, 57, 5-6, 412-430, 2010. doi
1047 10.1016/j.dsr2.2009.08.021.
1048 Matos, L., Mienis, F., Wienberg, C., Frank, N., Kwiatkowski, C., Groeneveld, J., Thil, F., Abrantes, F., Cunha, M.R.,
1049 and Hebbeln, D.: Interglacial occurrence of cold-water corals off the Cape Lookout (NW Atlantic): First
1050 evidence of the Gulf Stream influence, Deep-Sea Res Pt I, 105, 158-170, 2015.
1051 Matos, L., Wienberg, C., Titschack, J., Schmiedl, G., Frank, N., Abrantes, F., Cunha, M.R., and Hebbeln, D.: Coral
1052 mound development at the Campeche cold-water coral province, southern Gulf of Mexico: Implications of
1053 Antarctic Intermediate Water increased influence during interglacials, Mar Geol, 392, 53-65, 2017.

https://doi.org/10.5194/cp-2021-162
Preprint. Discussion started: 14 January 2022

1054 McCave, I.N. and Hall, I.R.: Size sorting in marine muds: Processes, pitfalls, and prospects for paleoflow-speed
1055 proxies, Geochem Geophy Geosy, 7, 2006.
1056 McCave, I.N., Manighetti, B., and Robinson, S.G.: Sortable silt and fine sediment size/composition slicing:
1057 Parameters for palaeocurrent speed and palaeoceanography, Paleoceanography, 10, 593-610, 1995.
1058 McCave, I.N., Thornalley, D.J.R., and Hall, I.R.: Relation of sortable silt grain-size to deep-sea current speeds:
1059 Calibration of the 'Mud Current Meter', Deep-Sea Res Pt I, 127, 1-12, 2017.
1060 Mienis, F., Duineveld, G.C.A., Davies, A.J., Ross, S.W., Seim, H., Bane, J., and can Weering, T.C.E.: The influence
1061 of near-bed hydrodynamic conditions on cold-water corals in the Viosca Knoll area, Gulf of Mexico, Deep-Sea
1062 Res Pt I, 60, 32-45, 2012.
1063 Mienis, F., de Stigter, H.C., White, M., Duineveld, G., de Haas, H., and van Weering, T.C.E.: Hydrodynamic
1064 controls on cold-water coral growth and carbonate-mound development at the SW and SE Rockall Trough
1065 Margin, NE Atlantic Ocean, Deep-Sea Res Pt I, 54, 1655-1674, 2007.
1066 Mienis, F., van der Land, C., de Stigter, H.C., van de Vorstenbosch, M., de Haas, H., Richter, T., van Weering,
1067 T.C.E.: Sediment accumulation on a cold-water carbonate mound at the Southwest Rockall Trough margin, Mar
1068 Geol 265, 40-50, 2009.
1069 Milker, Y., Schmiedl, G., Betzler, C., Römer, M., Jaramillo-Vogel, D., and Siccha, M.: Distribution of recent benthic
1070 foraminifera in shelf carbonate environments of the Western Mediterranean Sea, Mar Micropaleontol, 73, 207-
1071 225, 2009.
1072 Millot, C.: Circulation in the western Mediterranean Sea, J Marine Syt, 20, 423-442, 1999.
1073 Millot, C.: Another description of the Mediterranean Sea outflow, Prog Oceanogr, 82, 101-124, 2009.
1074 Millot, C.: Levantine Intermediate Water characteristics: an astounding general misunderstanding!, Sci Mar, 77, 217-
1075 232, 2013.
1076 Millot, C., Candela, J., Fuda, J.-L., and Tber, Y.: Large warming and salinification of the Mediterranean outflow due
1077 to changes in its composition, Deep-Sea Res Pt I, 53, 656-666, 2006.
1078 Mohn, C., Rengstorf, A., White, M., Duineveld, G., Mienis, F., Soetaert, K., and Grehan, A.: Linking benthic
1079 hydrodynamics and cold-water coral occurrences: A high-resolution model study at three cold-water coral
1080 provinces in the NE Atlantic, Prog Oceanogr, 122, 92-104, 2014.
1081 Mojtahid, M., Jorissen, F., Lansard, B., Fontanier, C., Bombled, B., and Rabouille, C.: Spatial distribution of live
1082 benthic foraminifera in the Rhône prodelta: Faunal response to a continental–marine organic matter gradient,
1083 Mar Micropaleontol, 70, 177-200, 2009.
1084 Murray, J.W.: Ecology and Applications of Benthic Foraminifera, Cambridge University Press, 2006.
1085 Negri, M.P. and Corselli, C.: Bathyal *Mollusca* from the cold-water coral biotope of Santa Maria di Leuca (Apulian
1086 margin, southern Italy), Zootaxa, 4186, 2016.
1087 Olivet, J.L., Auzende, J.M., and Bonnin, J.: Structure et évolution tectonique du bassin d'Alboran, B Soc Geol Fr, 7,
1088 491-495, 1973.
1089 Osborne, A.H., Vance, D., Rohling, E.J., Barton, N., Rogerson, M., and Fello, N.: A humid corridor across the
1090 Sahara for the migration of early modern humans out of Africa 120,000 years ago, PNAS 105, 16444-16447,
1091 2008.

https://doi.org/10.5194/cp-2021-162
Preprint. Discussion started: 14 January 2022


Climate of the Past Discussions

1092 Paillard, D., Labeyrie, L., Yiou, P.: Macintosh Program performs time Series Analysis, EOS Trans. AGU, 77.
1093 http://www.agu.org/eos_elec/96097e.html, 1996.
1094 Pasquier, V., Toucanne, S., Sansjofre, P., Dixit, Y., Revillon, S., Mokeddem, Z., and Rabineau, M.: Organic matter
1095 isotopes reveal enhanced rainfall activity in Northwestern Mediterranean borderland during warm substages of
1096 the last 200 ky, Quaternary Sci Rev, 205, 182-192, 2018
1097 Pérez-Folgado, M., Sierro, F.J., Flores, J.A., Grimalt, J.O., and Zahn, R.: Paleoclimatic variations in foraminifer
1098 assemblages from the Alboran Sea (Western Mediterranean) during the last 150 ka in ODP Site 977, Mar Geol,
1099 212, 113-131, 2004.
1100 Phleger, F.B. and Soutar, A.: Production of Benthic Foraminifera in Three East Pacific Oxygen Minima,
1101 Micropaleontology, 19, 110-115, 1973.
1102 Pomar, L., Morsilli, M., Hallock, P., and Bádenas, B.: Internal waves, and under-explored source of turbulence
1103 events in the sedimentary record, Earth Sci Rev, 111, 56-81, 2012.
1104 R Core Team.: R: A language and environment for statistical computing, R Foundation for Statistical Computing,
1105 Vienna, Austria, URL https://www.R-project.org/., 2018
1106 Rabineau, M., Berné, S., Olivet, J-L., Aslanian, D., Guillocheau, F., and Joseph, P.: Paleo sea levels reconsidered
1107 from direct observation of paleoshoreline position during Glacial Maxima (for the last 500,000 yr), Earth Planet
1108 Sc Lett, 252, 119-137, 2006.
1109 Rachid, J., Hssaida, T., Hamoumi, N., Terhzaz, L., Spezzaferri, S., Frank, N., and Daghor, L.: Palynological study of
1110 carbonated mounds during the Holocene along the Atlantic and Mediterranean Moroccan margins, Rev
1111 Palaeobot and Palyno, 278, 104213, 2020
1112 Raddatz, J., Rüggeberg, A., Flögel, S., Hathorne, E.D., Liebetrau, V., Eisenhauer, A., and Dullo, W-C.: The
1113 influence of seawater pH on U/Ca ratios in the scleractinian cold-water coral *Lophelia pertusa*, Biogeosciences,
1114 7, 1863-1871, 2014.
1115 Ramsey, C.: OxCal 4.2.4, Electronic document, URL https://c14.arch.ox.ac.uk/oxcal.html., 2017.
1116 Reimer, P.J., Bard, E., Bayliss, A., Beck, J.W., Blackwell, P.G., Ramsey, C.B., Buck, C.E., Cheng, H., Edwards,
1117 R.L., Friedrich, M., Grootes, P.M., Guilderson, T.P., Haflidason, H., Hajdas, I., Hatté, C., Heaton, T.J.,
1118 Hoffmann, D.L., Hogg, A.G., Hughen, K.A., Kaiser, K.F., Kromer, B., Manning, S.W., Niu, M., Reimer, R.W.,
1119 Richards, D.A., Scott, E.M., Southon, J.R., Staff, R.A., Turney, C.S.M., and van der Plicht, J.: IntCal13 and
1120 Marine13 Radiocarbon Age Calibration Curves 0–50,000 Years cal BP, Radiocarbon, 55, 1869-1887, 2013.
1121 Roberts, J.M., Wheeler, A.J., and Freiwald, A.: Reefs of the Deep: The Biology and Geology of Cold-Water Coral
1122 Ecosystems, Science, 312, 543-547, 2006.
1123 Roberts, J.M., Wheeler, A.J., Freiwald, A., and Cairns, S.: Cold-Water Corals, Cambridge University Press, 351 pp.,
1124 2009.
1125 Rodrigo-Gámiz, M., Martínez-Ruiz, F., Jiménez-Espejo, F.J., Gallego-Torres, D., Nieto-Moreno, V., Romero, O.,
1126 Ariztegui, D.: Impact of climate variability in the western Mediterranean during the last 20,000 years: oceanic
1127 and atmospheric responses. Quaternary Science Reviews, 30, 2018-2034, 2011.

https://doi.org/10.5194/cp-2021-162
Preprint. Discussion started: 14 January 2022

1128 Rogerson, M., Dublyansky, Y., Hoffmann, D.L., Luetscher, M., Spötl, C., and Töchterle, P.: Enhanced
1129 Mediterranean water cycle explains increased humidity during MIS 3 in North Africa, Clim Past Discussions, 1-
1130 31, 2018.
1131 Rohling, E.J., Cane, T.R., Cooke, S., Sprovieri, M., Bouloubassi, I., Emeis, K.C., Schiebel, R., Kroon, D., Jorissen,
1132 F.J., Lorre, A., and Kemp, A.E.S.: African monsoon variability during the previous interglacial maximum, Earth
1133 Planet Sc Lett, 202, 61-75, 2002.
1134 Rüggeberg, A., Dullo, C., Dorschel, B., and Hebbeln, D.: Environmental changes and growth history of a cold-water
1135 carbonate mound (Propeller Mound, Porcupine Seabight), Int J Earth Sci, 96, 57-72, 2007.
1136 Schiebel, R. and Hemleben, C.: Planktic Foraminifers in the Modern Ocean, Springer-Verlag, Berlin, Heidelberg,
1137 358 pp., 2017.
1138 Schmiedl, G., De Bovée, F., Buscail, R., Charriere, B., Hemleben, C., Medernach, L., and Picon, P.: Trophic control
1139 of benthic foraminiferal abundance and microhabitat in the bathyal Gulf of Lions, western Mediterranean Sea,
1140 Mar Micropaleontol, 40, 167-188, 2000.
1141 Schmiedl, G., Kuhnt, T., Ehrmann, W., Emeis, K.-C., Hamann, Y., Kotthoff, U., Dulski, P., and Pross, J.: Climatic
1142 forcing of eastern Mediterranean deep-water formation and benthic ecosystems during the past 22 000 years,
1143 Quaternary Sci Rev, 29, 3006-3020, 2010.
1144 Scholz, J. and Hillmer, G.: Reef-Bryozoans and Bryozoan-Microreefs: Control Factor Evidence from the Philippines
1145 and other Regions, Facies, 32, 109-144, 1995.
1146 Shanahan, T.M., McKay, N.P., Hughen, K.A., Overpeck, J.T., Otto-Bliesner, B., Heil, C.W., Scholz, C.A., and Peck,
1147 J.: The time-transgressive termination of the African Humid Period, Nat Geosci, 8, 140-144, 2015.
1148 Siani, G., Paterne, M., Arnold, M., Bard, E., Métivier, B., Tisnérat-Laborde, N., and Bassinot, F.: Radiocarbon
1149 reservoir ages in the Mediterranean Sea and Black Sea, Radiocarbon, 42, 2, 271-280, 2000.
1150 Sierro, F.J., Hodell, D.A., Curtis, J.H., Flores, J.A., Reguera, I., Colmenero-Hidalgo, E., Bárcena, M.A., Grimalt,
1151 J.O., Cacho, I., Frigola, J., and Canals, M.: Impact of iceberg melting on Mediterranean thermohaline circulation
1152 during Heinrich events, Paleoceanography, 20, 2005.
1153 Snousi, M.: Review of Certain Basic Elements for the Assessment of Environmental Flows in the Lower Moulouya,
1154 IUCN International Union for Conservation of Nature, Gland, Switzerland, 2004. Available online:
1155 http://cmsdata.iucn.org/downloads/morocco.pdf (accessed on 20 August 2012).
1156 Sparnocchia, S., Picco, P., Manzella, G., Ribotti, A., Copello, S., and Brasey, P.: Intermediate water formation in the
1157 Ligurian Sea, Oceanol Acta, 18, 151-162, 1995.
1158 Spezzaferri, S., Rüggeberg, A., Stalder, C., and Margreth, S.: Benthic foraminiferal assemblages from cold-water
1159 coral ecosystems, in: Atlas of Benthic Foraminifera From Cold-Water Coral Reefs, edited by: Spezzaferri, S.,
1160 Rüggeberg, A., and Stalder, C., Special Publication/Cushman Foundation For Foraminiferal Research, 20-48,
1161 2014.
1162 Spötl C. and Vennemann T.W.: Continuous-flow IRMS analysis of carbonate minerals, Rapid Commun Mass Sp,
1163 17, 1004-1006, 2003.
1164 Stalder, C., El Kateb, A., Vertino, A., Rüggeberg, A., Camozzi, O., Pirkenseer, C.M., Spangenberg, J.E., Hajdas, I.,
1165 Van Rooij, D., and Spezzaferri, S.: Large-scale paleoceanographic variations in the western Mediterranean Sea

https://doi.org/10.5194/cp-2021-162
Preprint. Discussion started: 14 January 2022

during the last 34,000 years: From enhanced cold-water coral growth to declining mounds, Mar Micropaleontol, 143, 46-62, 2018.

Stalder, C., Vertino, A., Rosso, A., Ruggeberg, A., Pirkenseer, C., Spangenberg, J.E., Spezzaferri, S., Camozzi, O., Rappo, S., and Hajdas, I.: Microfossils, a Key to Unravel Cold-Water Carbonate Mound Evolution through Time: Evidence from the Eastern Alboran Sea, PLoS One, 10, e0140223, 2015.

Suhr, S.B., Pond, D.W., Gooday, A.J., and Smith, C.R.: Selective feeding by benthic foraminifera on phytodetritus on the western Antarctic Peninsula shelf: Evidence from fatty acid biomarker analysis, Mar Ecol Prog Ser, 262, 153-162, 2003.

Sun, X., Corliss, B.H., Brown, C.W., and Showers, W.J.: The effect of primary productivity and seasonality on the distribution of deep-sea benthic foraminifera in the North Atlantic, Deep-Sea Res Pt I, 53, 28-47, 2006.

Synal, H.A., Stocker, M., and Suter, M.: MICADAS: A new compact radiocarbon AMS system, Nucl Instrum Meth B, 259, 7-13, 2007.

Talbot, M.R. and Livingstone, D.A.: Hydrogen index and carbon isotopes of lacustrine organic matter as lake level indicators, Palaeogeogr Palaeocl, 70, 121-137, 1989.

Tekken, V. and Kropp, J.P.: Climate-driven or human-induced; indicating severe water scarcity in the Moulouya River basin (Morocco), Water, 4, 959-982, 2012.

Terhzaz, L., Hamoumi, N., Spezzaferri, S., El Mostapha L., and Henriet, J.P.: Carbonate mounds of the Moroccan Mediterranean margin: Facies and environmental controls, C R Geosci, 350, 212–221. 2018.

Titschak, J., Thierens, M., Dorschel, B., Schulbert, C., Freiwald, A., Kano, A., Takashima, C., Kawagoe, N., Li, X., and IODP Expedition 307 scientific party: Carbonate budget of a cold-water coral mound (Challenger Mound, IODP Exp. 307), Mar Geol, 259, 36-46, 2009.

Toucanne, S., Jouet, G., Ducassou, E., Bassetti, M.-A., Dennielou, B., Angue Minto'o, C.M., Lahmi, M., Touyet, N., Charlier, K., Lericolais, G., and Mulder, T.: A 130,000-year record of Levantine Intermediate Water flow variability in the Corsica Trough, western Mediterranean Sea, Quaternary Sci Rev, 33, 55-73, 2012.

Tuenter, E., Weber, S.L., Hilgen, F.J., and Lourens, L.J.: The response of the African summer monsoon to remote and local forcing due to precession and obliquity, Global Planet. Change, 36, 219-235, 2003.

Van Krevelen, D.W.: Coal: typology–physics–chemistry–constitution, 3rd edition, Elsevier Science Publishers, 1993.

Van Rooij, D., Hebbeln, D., Comas, M., Vandorpe, T., Delivet, S., and the shipboard scientific party,: EUROFLEETS Cruise Summary Report, The Mediterranean-Atlantic Gateway Code: The Late Pleistocene Carbonate Mound Record, 2013.

Viúdez, Á. and Tintoré, J.: Time and space variability in the Eastern Alboran Sea from March to May 1990, J Geophys Res, 100, 1995.

Wang, H., Lo Iacono, C., Wienberg, C., Titschack, J., and Hebbeln, D.: Cold-water coral mounds in the southern Alboran Sea (western Mediterranean Sea): Internal waves as an important driver for mound formation since the last deglaciation, Mar Geol, 412, 1-18, 2019.

https://doi.org/10.5194/cp-2021-162
Preprint. Discussion started: 14 January 2022


Climate of the Past Discussions

1202 Wefing, A.-M., Arps, J., Blaser, P., Wienberg, C., Hebbeln, D., and Frank, N.: High precision U-series dating of
1203 scleractinian cold-water corals using an automated chromatographic U and Th extraction, Chem Geol, 475, 140-
1204 148, 2017.
1205 Wehrmann, L.M., Knab, N.J., Pirlet, H., Unnithan, V., Wild, C., and Ferdelman, T.G.: Carbon mineralization and
1206 carbonate preservation in modern cold-water coral reef sediments on the Norwegian shelf, Biogeosciences, 6,
1207 663-680, 2009.
1208 White, M.: Benthic dynamics at the carbonate mound regions of the Porcupine Sea Bight continental margin, Int J
1209 Earth Sci96, 1-9, 2007.
1210 White, M., Mohn, C., De Stigter, H.C., and Mottram, G.: Deep-water coral development as a function of
1211 hydrodynamics and surface productivity around the submarine banks of the Rockall Trough, NE Atlantic, in:
1212 Cold-water Corals and Ecosystems, edited by: Freiwald, A. and Roberts, J.M., Springer-Verlag, Berlin,
1213 Heidelberg, 503-514 pp., 2005.
1214 Wickham, H.: ggplot2: Elegant Graphics for Data Analysis, Springer-Verlag, New York, 2016.
1215 Wienberg, C. A deglacial cold-water coral boom in the Alboran Sea: From coral mounds and species dominance, in:
1216 Mediterranean cold-water corals: past, present and future, edited by: Orejas, C. and Jiménez, C., Springer, 57-
1217 60, 2019.
1218 Wienberg, C. and Titschak, J.: Framework-forming scleractinian cold-water corals through space and time: a Late
1219 Quaternary North Atlantic perspective, in: Marine Animal Forests, edited by: Rossi, S., Springer, Switzerland,
1220 2015.
1221 Wienberg, C., Hebbeln, D., Fink, H.G., Mienis, F., Dorschel, B., Vertino, A., Correa, M.L., and Freiwald, A.:
1222 Scleractinian cold-water corals in the Gulf of Cádiz—First clues about their spatial and temporal distribution,
1223 Deep-Sea Res Pt I, 56, 1873-1893, 2009.
1224 Wienberg, C., Titschack, J., Frank, N., De Pol-Holz, R., Fietzke, J., Eisele, M.H., Kremer, A., Hebbeln, D.: Deglacial
1225 upslope shift of NE Atlantic intermediate waters controlled slope erosion and cold-water coral mound
1226 formation (Porcupine Seabight, Irish margin). Quaternary Science Reviews, 237, 106310, 2020.
1227 Wienberg, C., Titschack, J., Freiwald, A., Frank, N., Lundälv, T., Taviani, M., Beuck, L., Schröder-Ritzrau, A.,
1228 Krengel, T., Hebbeln, D.: The giant Mauritanian cold-water coral mound province: Oxygen control on coral
1229 mound formation, Quaternary Sci Rev, 185, 135-152, 2018.
1230 Wilson, J.B.: 'Patch' development of the deep-water coral *Lophelia Pertusa* (L.) on Rockall Bank, J Mar Biol Assoc
1231 UK, 59, 1979.
1232 Winston, J.E.: Feeding in marine bryozoans, in Biology of Bryozoans, edited by: Woollacott, R.M. and Zimmer,
1233 R.L., 233–271 pp., Academic, San Diego, Calif., 1977.
1234 Winston, J. E.: Feeding behaviour of modern bryozoans, in Lophophorates: Notes for a Short Course, Stud. Geol.,
1235 vol. 5, edited by: Broadhead, T.W., 1–21 pp., Univ. of Tenn., Knoxville, 1981.